

Conventional and Unconventional Photon Statistics

Eduardo Zubizarreta Casalengua, Juan Camilo López Carreño, Fabrice P. Laussy, and Elena del Valle*

The photon statistics emitted by a large variety of light-matter systems under weak coherent driving can be understood, to lowest order in the driving, in the framework of an admixture of (or interference between) a squeezed state and a coherent state, with the resulting state accounting for all bunching and antibunching features. One can further identify two mechanisms that produce resonances for the photon correlations: i) conventional photon blockade describes cases that involve a particular quantum level or set of levels in the excitation/emission processes with interferences occurring to all orders in the photon numbers, while ii) unconventional photon blockade describes cases where the driving laser is far from resonance with any level and the interference occurs for a particular number of photons only, yielding stronger correlations but only for a definite number of photons. Such an understanding and classification allows for a comprehensive and transparent description of the photon statistics from a wide range of disparate systems, where optimum conditions for various types of photon correlations can be found and realized.

across different platforms for its practicality of operation (with a laser) and appealing underlying mechanism.^[5–13] This so-called “blockade” effect describes how the occupation of an energy level by a particle forbids another particle to occupy the same level. As such, it is reminiscent of Pauli’s exclusion principle^[14,15] and indeed the first type of blockade involved electrons in the so-called “Coulomb blockade.”^[16–18] While Pauli’s principle relies on the antisymmetry of fermionic wavefunctions, one can also implement a blockade from repulsive interactions of the excitations created when driving the system, as neatly illustrated with alkali atoms excited to high principal quantum numbers (Rydberg states), giving rise to Rydberg blockade from the strong dipole repulsion.^[19,20] In this framework, the underlying medium can

1. Blockade in Quantum Optics

Quantum optics was born with the study of photon statistics.^[1] Following Hanbury Brown’s discovery of photon bunching^[2,3] and Kimble et al.’s observation of antibunching,^[4] there has been a burgeoning activity of tracking how pairs of detected photons are related to each other. From the various mechanisms that generate correlated photons, one that turns an uncorrelated stream into antibunched photons has attracted much attention

even be bosonic and broadly described as an anharmonic oscillator^[21–23] with the blockade arising from nonlinearities in the energy levels. The idea is simple: when the exciting photons are resonant with the bare frequency of the oscillator, a first photon can excite the system, but due to the system’s interactions, a subsequent photon is now detuned from the oscillator’s frequency. If its energy is not sufficient to climb the ladder of states, it cannot excite the system, that thus remains with one photon only. In this way, one can turn a coherent—that is, uncorrelated when measured—stream of photons, with its characteristic Poissonian fluctuations, into a more ordered stream of separated photons, effectively acting as a “photon turnstile.”^[7,8,11] The quality of such a suppression of the photon clumping can be measured at the two-photon level with Glauber’s second-order correlation function $g^{(2)}(\tau)$, that compares the coincidences in time to those expected from a random process of same intensity. Correlations decrease from 1, with no blockade, toward 0 as the nonlinearity U increases. In the limit where U becomes infinite, putting the second excited state arbitrarily far and realizing a two-level system (2LS), a second photon is strictly forbidden and $g^{(2)}$ becomes perfectly antibunched. For open bosonic systems, the ratio of the interaction to the decay rate is an important variable for the blocking to be effective. The “blockade” regime is reached when interactions overtake dissipation.^[24] This can be marked as the onset of antibunching: one photon starts to suppress the next one.

The driven damped anharmonic system is an important model, not least because it is one of the few cases to enjoy an exact analytical solution.^[25] While much of the mechanism is contained in this particular case, compound systems—where the anharmonic system is coupled to a single-mode cavity—have also attracted considerable attention. This describes for instance

E. Zubizarreta Casalengua, Dr. J. C. López Carreño, Dr. E. del Valle
Departamento de Física Teórica de la Materia Condensada and
Condensed Matter Physics Center (IFIMAC)
Universidad Autónoma de Madrid
Madrid 28049, Spain

E-mail: elena.delvalle.reboul@gmail.com; elena.delvalle@uam.es

E. Zubizarreta Casalengua, Dr. J. C. López Carreño, Prof. F. P. Laussy,
Dr. E. del Valle


Faculty of Science and Engineering
University of Wolverhampton

Wulfruna St, Wolverhampton WV1 1LY, UK

Prof. F. P. Laussy

Russian Quantum Center

Novaya 100, Skolkovo, Moscow 143025, Russia

 The ORCID identification number(s) for the author(s) of this article can be found under <https://doi.org/10.1002/lpor.201900279>

© 2020 The Authors. Published by WILEY-VCH Verlag GmbH & Co. KGaA, Weinheim. This is an open access article under the terms of the Creative Commons Attribution License, which permits use, distribution and reproduction in any medium, provided the original work is properly cited.

DOI: 10.1002/lpor.201900279

interacting quantum-well excitons coupled to a microcavity mode.^[26] The effect is then known as “polariton-blockade,” after the eponymous light–matter particles that constitute the elementary excitations of such systems. This configuration was first addressed theoretically by Verger et al.^[27] for exciton–polaritons. They studied the response of the cavity around the lower-polariton resonance, predicting antibunching indeed, although of too small magnitude with the parameters of typical systems to be observed easily. This spurred interest in polariton boxes and other ways of confining polaritons to enhance their interactions.^[28] Much progress has since been made in boosting polariton interactions, for example, with dipolar polaritons^[29,30] or with collective Rydberg excitation of a laser-cooled atomic ensemble.^[31] Nonetheless, Liew and Savona had computed a much stronger antibunching in coupled cavities than is allowed by polariton blockade with the same order of weak nonlinearity.^[32] This so-called “unconventional polariton blockade” was quickly understood as originating not from the particular configuration of coupled cavities with weak Kerr nonlinearities but from a subtler type of blocking, due to destructive interferences between probability amplitudes whenever there are two paths that can reach the excited state with two photons.^[33] This result has generated considerable attention, although it was later remarked^[34] that it was a known effect,^[35,36] observed decades earlier^[37] where it received a much smaller followup. Besides, Lemonde et al.^[34] further clarified how unconventional photon blockade is connected to squeezing rather than single-photon states, which had been presented as one of the main interest of the effect. Recently, both conventional^[38,39] and unconventional^[40,41] blockades have been reported in solid-state systems, where the 2010 revival of the idea had triggered intense activity.

In this text, we provide a unifying picture of the two types of polariton blockades. We show how they typically sit next to each other in interacting coupled light–matter systems along with other phenomenologies that produce superbunching instead of the blockade antibunching. In particular, we show that they are both rooted in the single-component system, either a 2LS or an anharmonic oscillator, with strong photon correlations produced by interfering the emitter’s incoherent signal with a coherent fraction. We will nevertheless highlight how the two blockades are intrinsically different mechanisms with different characteristics. Most importantly, the conventional blockade, based on dressed-state blocking, yields photon antibunching at all orders in the number of photons, that is, $g^{(N)} \rightarrow 0$ for all $N \geq 2$, while the unconventional blockade can only target one N in isolation, producing bunching for the others. Another apparent similarity is that both types of blockades produce the same state in what concerns the population and the two-photon correlation $g^{(2)}$ at the lowest order in the driving, but differences occur at higher orders, namely, at the second-order in the driving for $g^{(2)}$ and at the third-order for the population. Differences exist already at the lowest order in the driving for $g^{(3)}$ and higher-order photon correlations, making it clear that the two mechanisms differ substantially and produce different states, despite strong resemblances in the quantities of easiest experimental reach. The state produced by both types of blockade at the two-photon level results from a simple interference between a squeezed state and a coherent state. While the squeezing is typically produced by the emitter, the co-



Eduardo Zubizarreta Casalegna is a Ph.D. student at the Universidad Autónoma de Madrid (UAM), Spain, and the University of Wolverhampton (UK), working on the dynamics of quantum correlations in open quantum systems and the theory of multiphoton light.



Juan Camilo López Carreno studied for his undergraduate degree from Bogotá (Colombia) with research experience in Madrid and Lecce (Italy). He obtained his Ph.D. from UAM, in 2019, on the topic of exciting optical targets with quantum light, and is currently a lecturer and research associate at the University of Wolverhampton.



Fabrice Laussy received his Ph.D. from the Université Blaise Pascal in Clermont-Ferrand, France, in 2005, with subsequent postdoctoral work in Sheffield, Madrid, Munich (Marie Curie) & Ramón y Cajal tenure (UAM). He is currently at the Russian Quantum Center and chair of light–matter interactions at the University of Wolverhampton.



Elena del Valle obtained her Ph.D. from the UAM, in 2009. She toured Europe with prestigious fellowships (Newton in Southampton, Humboldt in Munich, Marie Curie in Madrid) with Ramón y Cajal tenure (UAM) in 2015, and is currently a senior lecturer in quantum optics at the University of Wolverhampton.

herent fraction can be either brought from outside, idoneously, as a fraction of the driving laser itself—a technique known as “homodyning”—or be produced internally by the driven system itself, a concept introduced in the literature under the apt qualification of “self-homodyning.”^[35] We will thus highlight that, to this order, essentially the same physics—of tailoring two-photon

statistics by admixing squeezed and coherent light, discussed in Section 3—takes place in a variety of platforms, overviewed in Section 2. We will further synthesize this picture by unifying the cases where the nonlinearity is: i) strong, namely, provided by a 2LS (Section 4) or on the contrary ii) weak, namely, provided by an anharmonic oscillator (Section 5), and how these are further generalized in presence of a cavity where self-homodyning becomes a compelling picture since a cavity is an ideal receptacle for coherent states. This brings the 2LS into the Jaynes–Cummings model (Section 6) and the anharmonic oscillator into microcavity polaritons (Section 7), respectively. There are many variations in between all these configurations, that the literature has touched upon in many forms, as we briefly overview in the next section. For our own discussion, while we have tried to retain generality for the variables that play a significant role, we do not include for the sake of brevity all the possible combinations, which could of course be done would the need arise for a given platform. Instead, we briefly consider features common to all these cases regarding their response to dephasing (Section 8) and found in their time-dependence (Section 9), before discussing (Section 10) and concluding (Section 11).

2. The Blockade Hamiltonian

A fairly general type of photon blockade is described by the following Hamiltonian:

$$H = \hbar\omega_a a^\dagger a + \hbar\omega_b b^\dagger b + \hbar g(a^\dagger b + ab^\dagger) + \frac{U_a}{2} a^\dagger a^\dagger a a + \frac{U_b}{2} b^\dagger b^\dagger b b + \Omega_a e^{i\omega_a t} a + \Omega_b e^{i\omega_b t} b + \text{h.c.} \quad (1)$$

where $\hbar\omega_c$ is the free energy of the modes $c = a, b$, both bosonic; $\hbar g$ describes their Rabi coupling, giving rise to polaritons as eigenstates of the 1st line of Equation (1); U_c are the nonlinearities of the respective modes, here again for $c = a, b$; and Ω_c describes resonant excitation at the energy ω_c . Some details of the microscopic derivation can be found in ref. [27]. This is brought to the dissipative regime through the standard techniques of open quantum systems, namely, with a master equation in the Lindblad form $\partial_t \rho = i[\rho, H] + \sum_{c=a,b} (\gamma_c/2) \mathcal{L}_c \rho$, where the superoperator $\mathcal{L}_c \rho \equiv 2c\rho c^\dagger - c^\dagger c \rho - \rho c^\dagger c$ describes a decay rate of mode c at rate γ_c (dephasing is dealt with separately in Section 8). Particular cases or variations of Equation (1) have been studied in numerous works, even when restricting to those with a focus on the emitted photon statistics. This ranges from cases retaining one mode only^[42] to the most general form of Equation (1).^[43–48] Regarding the central theme of this work of field-admixture, a first consideration on the photon statistics of the effect of interfering a quantum signal with a coherent field was made by Flyach and Savona,^[45] who found that the conditions for strong correlations are shifted rather than hampered. This touches upon, in the framework of input/output theory, the mechanisms of mixing fields that we will highlight in the following, where we will show that beyond being altered, correlations can be drastically optimized (becoming exactly zero to first order for antibunching and infinite for bunching). In a later work,^[46] they further progressed toward fully exploiting homodyning by including

a “dissipative, one-directional coupling” term, which allowed them to achieve a considerable improvement of the photon correlations, especially in time, with suppression of oscillations and the emergence of a plateau at small time delays (discussed in Section 9). This mechanism has been singled-out and optimized in a different context^[49] (a two-level system admixed to an external laser). Credit for quantum-classical field admixtures should also be given to the bulk of work devoted to these ideas by the Vucković group, starting with their use of self-homodyning to study the Mollow triplet in a dynamical setting.^[50] Initially used as a suppression technique to access the quantum emitter’s dynamics by cancelling out the scattered coherent component from their driving laser,^[51,52] they later appreciated the widespread application of their effect and its natural occurrence in other systems,^[53] where it had passed unnoticed, as well as the benefits of a tunability of the interfering component,^[54] which they proposed in the form of a partially transmitting element in an on-chip integrated architecture that combines a waveguide with a quantum-dot/photonic-crystal cavity QED platform. Fischer et al.^[50,53] in particular started to develop and implement a series of pioneering contributions in the effect of homodyning for quantum engineering and optimization, which holds great promise for the future.^[55] In the following, we will provide the unified theory for such a mixing of coherent and quantum light. The possibility and benefits of an external laser to optimize photon correlations also appeared in a work by Van Regemortel et al.,^[56] with a foothold in the same ideas. The effect of tuning two types of driving was emphasized by Xu and Li,^[57] who reported among other notable results how changing their ratio can bring the system from strong antibunching to superbunching, an idea which we will revisit from the point of view of interfering fields through (controlled) homodyning or (self-consistent) self-homodyning. Snijders et al. used the interference to enhance bunching^[58] (and called it “purification”; we will call this “unconventional bunching”). Similar principles have then been explored and extended several times in many variations of the problem,^[59–75] which all fit nicely in the wider picture that we will present. In studying the same effect in different platforms, we will see it takes on seemingly different forms, with a deceiving tendency to exhibit specificities of the particular cases, such as following the characteristic level structures. Also, one manifestation only has been typically highlighted at a time, disconnected from the others or unaware of them. For instance, the microcavity–polariton configuration with interactions in one mode only (describing quantum well excitons, the other being a cavity mode) has been studied mainly from the (conventional) polariton blockade point of view,^[27,76] in which case, the (much stronger) unconventional antibunching has been largely overlooked. We will focus on the following on the one-interacting-mode case rather than on the possibly more popular two weakly interacting sites. First, because this allows a direct comparison with the Jaynes–Cummings limit, second, because this configuration became timely following the recent experimental breakthrough with polariton blockade.^[38,39] Other similar cases are also discussed in ref. [77]. Jaynes–Cummings blockade takes over polariton-blockade when the emitter is effectively a two-level system, that is, in platforms which exhibit very high nonlinearities, as is the case for instance with atoms, where photon-blockade and related effects were pioneered,^[9,78] or with molecules,^[79] thanks to the progresses in excitation and collection efficiency^[80] of a single-molecule

and the possibility to embed it in a microcavity, in which case antibunching and bunching of the type that we are about to describe have also been observed.^[81] The two-level system can also originate from a more complex environment, such as 0D excitations of a cloud of Rydberg atoms whose coupling to a cavity yield strongly-interacting dark polaritons,^[82] or so-called “artificial atoms” in the solid state, such as quantum dots^[41,83–85] or superconducting qubits.^[13,40,86] Whatever the platform, a similar physics of fields admixture repeatedly brings forward strong bunching and antibunching effects. This is true as well for other configurations that cannot be accommodated by Equation (1) in this form, or because they add even more components. One could mention examples from works that consider pulsed excitation,^[87,88] non-Markovian effects,^[89] that go beyond the rotating-wave approximation,^[90] involve additional modes (three in refs. [91–93]), different types of nonlinearity, for example, a^2 in ref. [94], $a^2 b^\dagger$ in refs. [95–97], $a^2 \sigma^\dagger$ in ref. [98], a four-level system in ref. [99]), two two-level systems in a cavity in ref. [100] and up to the general Tavis–Cummings model,^[101] pulsed coherent control of a two-level system in ref. [102], two coupled cavities each containing a two-level system^[103,104] up to a complete array.^[105,106] The phenomenology reported in each of these particular cases however falls within the classification that we will establish in the remaining of the text, that is, they can be understood as a homodyning effect of some sort. Finally, while several works have focused on single-photon emission as the spotlight for the effect (which is dubious when antibunching is produced from the unconventional route), others have also stressed different applications or suggested different contextualization, such as phase-transitions^[43] or entanglement,^[107] and there is certainly much to exploit from one perspective or another.^[108]

3. Homodyne and Self-Homodyne Interferences

We will return in the rest of this text to such systems as those discussed in the previous section—all a particular case or a variation of Equation (1)—to show that the two-photon statistics of their emission can be described to lowest order in the driving by a simple process: the mixing of a squeezed and a coherent state. In this section, we therefore study this configuration in details.

The mixing of two quantum fields is most simply achieved by passing them through the two ports of a balanced beam-splitter. In the homodyning case that involves a coherent state $|\alpha\rangle$, with complex amplitude $\alpha = |\alpha|e^{i\phi}$, mixed with a field of general nature, with annihilation operator d , the normally ordered correlators of the resulting field $s = \alpha + d$ is expressed in terms of the inputs as^[109]

$$\langle s^{\dagger n} s^m \rangle = \sum_{p=0}^n \sum_{q=0}^m \binom{n}{p} \binom{m}{q} \alpha^{*p} \alpha^q \langle d^{\dagger n-p} d^{m-q} \rangle \quad (2)$$

up to some unimportant normalization and phase-shift factors. In practice, the polarization degree of freedom is involved with one of the two optical polarizations used as the local oscillator, with a polarizer to mix them afterwards,^[58] but this needs not

enter our simple theoretical picture. From this expression, we can compute any relevant observable of the mixture. For instance, the total population is

$$\langle n_s \rangle \equiv \langle s^\dagger s \rangle = |\alpha|^2 + \langle n_d \rangle + 2\Re[\alpha^* \langle d \rangle] \quad (3)$$

with $n_d \equiv d^\dagger d$. Apart from the sum of both input intensities, there is a contribution (last term) from the first-order interference between the coherent components of each of the fields or mean fields. Similarly, the second-order coherence function, which is defined as

$$g_s^{(2)}(\tau) = \lim_{t \rightarrow \infty} \frac{\langle s^\dagger(t) (s^\dagger s)(t + \tau) s(t) \rangle}{[\langle s^\dagger s \rangle (t)]^2} = \frac{\langle s^\dagger (s^\dagger s)(\tau) s \rangle}{\langle n_s \rangle^2} \quad (4)$$

can be readily obtained from the correlators in Equation (2). We will restrict to steady-state situations (thus omitting t in all expressions) until Section 9 and will also set the delay $\tau = 0$, thus focusing on coincidences. This simplifies the notation $g_s^{(2)} = g_s^{(2)}(t \rightarrow \infty, \tau = 0)$. We will also consider N -th order coherence functions, also at zero delay: $g_s^{(N)} \equiv \langle s^{\dagger N} s^N \rangle / \langle s^\dagger s \rangle^N$. These correlators can always be written as a polynomial series of powers of the amplitude of the coherent field α .

$$g_s^{(N)} = \frac{\sum_{k=0}^{2N} c_k |\alpha|^k}{\langle n_s \rangle^N} \quad (5)$$

where c_k are coefficients that depend on the phase of the coherent field ϕ and mean values of the type $\langle d^{\mu} d^{\nu} \rangle$ with $\mu + \nu \leq N^2$. In particular, the 2nd-order correlation function, Equation (4), can be rearranged as

$$g_s^{(2)} = 1 + \mathcal{I}_0 + \mathcal{I}_1 + \mathcal{I}_2 \quad (6)$$

with $\mathcal{I}_m \sim |\alpha|^m$,^[35,110–112] where 1 represents the coherent contribution of the total signal, and the incoherent contributions read^[109]

$$\mathcal{I}_0 = \frac{\langle d^{\dagger 2} d^2 \rangle - \langle d^\dagger d \rangle^2}{\langle n_s \rangle^2} \quad (7a)$$

$$\mathcal{I}_1 = 4 \frac{\Re[\alpha^* (\langle d^\dagger d^2 \rangle - \langle d^\dagger d \rangle \langle d \rangle)]}{\langle n_s \rangle^2} \quad (7b)$$

$$\mathcal{I}_2 = \frac{\langle X_{d,\phi}^2 \rangle - \langle X_{d,\phi} \rangle^2}{\langle n_s \rangle^2} = \frac{(\Delta X_{d,\phi})^2}{\langle n_s \rangle^2} \quad (7c)$$

where $X_{d,\phi} = (e^{i\phi} d^\dagger + e^{-i\phi} d)/2$ is the quadrature with the same phase ϕ of the coherent field. Note that there are no explicit terms \mathcal{I}_3 and \mathcal{I}_4 because through simplifications these get absorbed in the first term (i.e., 1). This decomposition was first introduced by Carmichael^[35] and in fact precisely to show that the same quantum-optical phenomenology observed in different systems had the same origin, namely, to root nonclassical effects observed in optical bistability with many atoms in a cavity, to the physics of a single atom coherently driven, that is, resonance fluorescence. This is at this occasion of unifying squeezing and antibunching from two seemingly unrelated platforms under the

same umbrella of self-homodyning that he introduced this terminology. While these concepts have thus been invoked and explored from the earliest days of the field, it is only recently that they seem to start being fully understood and exploited, see for instance refs. [46, 49, 50, 53, 56]. Using such interferences to analyze the squeezing properties of a signal of interest (here, the field with annihilation operator d) through a controlled variation of a local oscillator (here, the coherent field α) was first suggested by Vogel,^[111,112] subsequently implemented to show squeezing in resonance fluorescence,^[113] and recently impulsed in a series of works from the Vucković group, as previously discussed. The physical interpretation of the contributions to the decomposition are as follows:

- The numerator of I_0 is the normally ordered variance of the signal intensity, that is, $\langle :(\Delta n_d)^2: \rangle = \langle :n_d^2: \rangle - \langle n_d \rangle^2$ with $n_d = d^\dagger d$ and $\Delta n_d = n_d - \langle n_d \rangle$. Therefore, $I_0 < 0$ indicates that the field d has sub-Poissonian statistics, which in turn contributes to the sub-Poissonian statistics of the total field s .
- The numerator of I_1 represents the normally ordered correlation between the fluctuation-field strength and intensity, $\langle d^\dagger d^2 \rangle - \langle d^\dagger d \rangle \langle d \rangle = \langle :\Delta d \Delta n_d: \rangle$, which have been referred to as anomalous moments^[111,112] and been recently measured.^[114] A squeezed-coherent state has such correlations.
- The numerator of I_2 is the variance of the quadratures of the field d . Having $I_2 < 0$ necessarily implies that the state of light has a squeezing component. This can be proved by noting that $:X_d^2: = X_d^2 - 1/4$ (the same for $:Y_d^2:$). If $I_2 < 0$, the standard deviation of $X_{d,\phi}$ must be less than $1/2$, but since $X_{d,\phi}$ and its orthogonal quadrature, $X_{d,\phi+\pi/2}$, must fulfil the Heisenberg uncertainty relation, $\Delta X_{d,\phi} \Delta X_{d,\phi+\pi/2} \geq 1/4$, then $\Delta X_{d,\phi+\pi/2} > 1/2$. This necessarily implies that there is a certain degree of squeezing in d . Nevertheless, the opposite statement is not true. A state with a non-zero degree of squeezing can have $I_2 \geq 0$, for instance, if the relative direction between the coherent and squeezing contributions fulfils $\theta - 2\phi = \pi/2$, where θ is the phase of the squeezing parameter (a straightforward example is provided by the displaced squeezed state). Furthermore, if $\langle d \rangle = 0$, the numerator of I_2 simplifies to $4|\alpha|^2 (\langle :X_d^2: \rangle - |\alpha|^2)$.

An analogous procedure likewise decomposes the higher-order coherence functions, that is, $g_s^{(n)} = 1 + \sum_{m=0}^{2n-2} \mathcal{J}_m^{(n)}$, with closed-form expressions for $\mathcal{J}_m^{(3)}$ given in ref. [109].

As an illustration which is at the heart of what follows, let us consider the interference of the coherent state with a squeezed state, as shown schematically in **Figure 1a**. The coherent state $|\alpha\rangle = D_a(\alpha)|0\rangle$ and the squeezed state $|\xi\rangle = S_d(\xi)|0\rangle$ are generated from a displacement $D_a(\alpha) = \exp(\alpha a^\dagger - \alpha^* a)$ and squeezing $S_d(\xi) = \exp(\frac{1}{2}[\xi d^{\dagger 2} - \xi^* d^2])$ operator, respectively, where $\xi = r e^{i\theta}$ is the squeezing parameter. Thus, the state that feeds the beam splitter is $|\psi_{in}\rangle = |\alpha, \xi\rangle = D_a(\alpha)S_d(\xi)|0\rangle_{da}$ where the state subscript indicates the input/output subspaces where operators are acting. The interference at the beam splitter mixes these two states. Writing the operators in the output basis gives^[109] $D_a(\alpha) = D_o(\alpha_o)D_s(\alpha_s) = D_s(\alpha_s)D_o(\alpha_o)$ where $\alpha_o = iR\alpha$, $\alpha_s = T\alpha$ and $D_j(\alpha_j) = \exp(\alpha_j j - \alpha_j^* j^\dagger)$ for $j = o, s$. Similarly, the

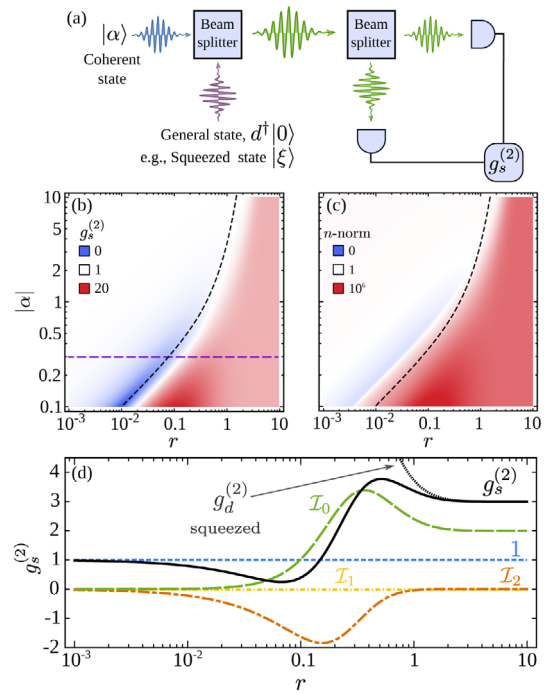


Figure 1. Second-order coherence function $g_s^{(2)}$ for the interference between a coherent and a quadrature-squeezed field, as in the setup shown in panel (a). The resulting $g_s^{(2)}$ is shown in panel (b) as a function of the coherent field $|\alpha|$ and squeezing parameter r (colour map in log scale). The relative phase ϕ between the squeezed and coherence state is the one that optimizes antibunching, that is, $\phi = \theta/2$. c) The n -norm (up to $g^{(6)}$, i.e., $n = 5$) as defined in Equation (18). Dashed black lines in both panels mark the minimum of $g_s^{(2)}$, showing that the best antibunching is no guarantee of good two-photon emission. d) Cut of $g_s^{(2)}$ along the horizontal dashed line in panel (b) ($|\alpha| = 0.3$) and its decomposition given by Equations (6) and (7). The black dotted line shows $g_d^{(2)}$ for the squeezed state only.

squeezing operator in the output basis reads:

$$S_d(\xi) = \exp \left[\frac{1}{2} (\xi_o^* o^2 - \xi_o o^{\dagger}) + \frac{1}{2} (\xi_s^* s^2 - \xi_s s^{\dagger}) + (\xi_{os}^* o s - \xi_{os} o^{\dagger} s^{\dagger}) \right] = \exp(S_o + S_s + S_{os}) \quad (8)$$

where $\xi_o = T^2 \xi$, $\xi_s = -R^2 \xi$ and $\xi_{os} = iRT \xi$. This exponential can be simply split into two different contributions only if $[S_o + S_s, S_{os}] = 0$, which is fulfilled in the particular case of a symmetric beam splitter ($T = R$); however, the first correction term grows proportionally to $r^2 \text{TR}(T^2 - R^2)$, so, for either low squeezing signal ($r \ll 1$) or almost symmetrical beam splitter ($T \approx R$), this is a good approximation. Besides, the commutator $[S_o, S_s]$ vanishes for any possible values, so the exponential simplifies to $S_d(\xi) = S_o(\xi_o)S_s(\xi_s)S_{os}(\xi_{os})$ and finally, the output state can be written as

$$|\psi_{out}\rangle = D_o(\alpha_o)S_o(\xi_o)D_s(\alpha_s)S_s(\xi_s)|\xi_{os}\rangle_{os} \quad (9)$$

where $|\xi_{os}\rangle = S_d(\xi)|0\rangle_{os} = \sum_n (\tanh r_{os})^n |n, n\rangle_{os} / \cosh r_{os}$ is a two-mode squeezed state^[115] with $r_{os} = |\xi_{os}| = RT r$. The signal of interest is obtained from the pure state $\rho_{out} = |\psi_{out}\rangle \langle \psi_{out}|$ by tracing out output o , $\rho_s = \text{Tr}_o\{\rho_{out}\}$. Using the cyclic properties of the

trace and the identities $D_o^\dagger(\alpha_o)D_o(\alpha_o) = S_o^\dagger(\xi_o)S_o(\xi_o) = \hat{1}_o$, where $\hat{1}_o$ is the identity operator, and since any operator that only acts on the s -subspace can be taken out of the trace, we find $\rho_s = D_s(\alpha_s)S_s(\xi_s)(\text{Tr}_o\{|\xi_{os}\rangle\langle\xi_{os}|\})S_s^\dagger(\xi_s)D_s^\dagger(\alpha_s)$ with the partial trace evaluating to

$$\rho_{\text{th}} \equiv \text{Tr}_o\{|\xi_{os}\rangle\langle\xi_{os}|\} = \frac{1}{\cosh^2 r_{os}} \sum_{n=0}^{\infty} (\tanh r_{os})^{2n} |n\rangle_s \langle n|_s \quad (10)$$

This has the form of a thermal state, with mean population $p_{\text{th}} \equiv \langle s^\dagger s \rangle = \sinh^2 r_{os}$. The output field detected at a single arm of the system therefore corresponds to a displaced squeezed thermal state. Finally,

$$\rho_s = D_s(\alpha_s)S_s(\xi_s)\rho_{\text{th}}S_s^\dagger(\xi_s)D_s^\dagger(\alpha_s) \quad (11)$$

with parameters $\alpha_s = T|\alpha|e^{i\phi}$, $\xi_s = r_s e^{i\theta_s} = R^2 e^{i(\theta+\pi)}$ and $p_{\text{th}} = \sinh^2(RT r)$. Even though T and R appear as general, the configuration of an interference assumes $R \approx T$. From now on, we consider the case of a 50:50 beam splitter ($T^2 = R^2 = 1/2$). The thermal population in terms of the squeezed population of the input signal $\langle n_d \rangle = \sinh^2 r$ becomes

$$p_{\text{th}} = \frac{1}{2}(\sqrt{1 + \langle n_d \rangle} - 1) \quad (12)$$

From ρ_s , one can compute the observables for the mixed signal, for example, $g_s^{(2)} = \text{Tr}[\rho_s s^{\dagger 2} s^2] / \text{Tr}[\rho_s s^\dagger s]^2$ ($g^{(3)}$ is given in ref. [109]):

$$\langle n_s \rangle = \frac{|\alpha|^2}{2} + \frac{\langle n_d \rangle}{2}, \quad | \langle s^2 \rangle | = \left(p_{\text{th}} + \frac{1}{2} \right) \sinh(r) \quad (13a)$$

$$g_s^{(2)} = 1 + \langle n_s \rangle^{-2} \sinh^2 r [\cosh 2r + 2|\alpha|^2 (1 - \cos(\theta - 2\phi) \coth r)] \quad (13b)$$

The second-order correlation for the total (13b) can be decomposed as in Equation (6) into

$$I_0 = \frac{\sinh[4](r)}{\langle n_s \rangle^2} [1 + \coth(r)^2], \quad I_1 = 0 \quad (14a)$$

$$I_2 = \frac{2|\alpha|^2 \sinh^2(r)}{\langle n_s \rangle^2} [1 - \cos(\theta - 2\phi) \coth(r)] \quad (14b)$$

where $\langle n_s \rangle = |\alpha|^2 + \sinh^2(r)$. Here, $\langle d \rangle = 0$ but also I_1 is exactly zero because, for a squeezed state, the correlators $\langle d^{\mu\nu} d^{\nu\mu} \rangle$ vanish when $\mu + \nu$ is an odd number. Useful expression for the decomposition of $g_s^{(2)}$ and $g_s^{(3)}$ in terms of the incoherent component and the two-photon coherence are given in ref. [109], where it is also shown how these states can be seen as steady-state solutions of a driven dissipative cavity, thus linking the dynamical parameters (such as the coherent driving and the squeezing intensity) to the abstract quantities α and r .

Inspection of Equation (14) shows that the only way in which $g_s^{(2)} < 1$, that is, the statistics of the total signal can be sub-Poissonian, regardless of the value of the squeezing parameter, is

for I_2 to be negative, which implies that the phases of the coherent state and the squeezing must be related by $|\theta - 2\phi| < \pi/2$. We take for simplicity the minimizing alignment, $\theta = 2\phi$, which means that the coherent and squeezed excitations are driven with the same phase, since the phase of the squeezed state is $\theta/2$. Using such a relation, the interference yields the correlation map shown in Figure 1b as a function of the amplitude of the coherent $|\alpha|$ and squeezing r intensities. The black dashed line shows the optimum amplitude of the coherent state that minimizes $g_s^{(2)}$ for a given squeezing, which is given by

$$|\alpha|_{\text{min}} = e^r \sqrt{\cosh(r) \sinh(r)} \quad (15)$$

Replacing this condition in Equations (14), we obtain the minimum possible value of $g_s^{(2)}$

$$g_{s, \text{min}}^{(2)} = 1 - \frac{e^{-2r}}{1 + \sinh(2r)} \leq 1 \quad (16)$$

This goes to zero although at the same time as the population goes to zero. Figure 1d shows a transverse cut of the correlation map in (b) along the purple long-dashed line, which corresponds to $|\alpha| = 0.3$. The decomposition and total $g_s^{(2)}$ are shown as a function of the squeezing parameter, with minimum $g_s^{(2)} = 0.26$ at $r \approx 0.078$. Without the interference with the coherent state, the squeezed state can never have sub-Poissonian statistics. In fact, in such a case, the correlations become independent of the phase of the squeezing parameter

$$g_d^{(2)} = g_s^{(2)}|_{\alpha \rightarrow 0} = 2 + \coth^2(r) \geq 3 \quad (17)$$

which is minimum when squeezing is infinite $r \rightarrow \infty$, and diverges at vanishing squeezing $r \rightarrow 0$, in which case the state is $|\xi\rangle = (1 - \frac{r^2}{4})|0\rangle - \frac{e^{i\theta} r}{\sqrt{2}}|2\rangle$ up to 2nd order, with vanishing signal $\langle n_d \rangle = \sinh^2(r)$.

There is a great tunability from such a simple admixture since $g_s^{(2)}$ of the light at the output of the beam splitter can be varied between 0 and ∞ simply by adjusting the magnitudes of the coherent field and the squeezing parameter. In particular, the most sub-Poissonian statistics occurs when coherent light interferes with a small amount of squeezing $r < |\alpha_{\text{min}}|$, in the right intensity proportion, given by Equation (15). Counter-intuitively, $g_s^{(2)} \ll 1$ occurs when the squeezed light itself is, on the opposite, super-Poissonian (even super-chaotic $g_d^{(2)} > 2$). For instance, in order to have $g_{s, \text{min}}^{(2)} < 1/2$, it is required that $r < \log(\sqrt{6} - 1)/2 \approx 0.186$,

which implies $g_d^{(2)} > 31.7$ and $|\alpha_{\text{min}}| > \sqrt{(2 - \sqrt{6})/2} \approx 0.52 > r$. This is a fundamental result that we will find throughout the text in order to find the conditions for and manipulate sub-Poissonian statistics and antibunching in various systems under weak coherent driving.

An important fact for our classification of photon statistics is that, since the sub-Poissonian behavior is here due to an interference effect, the set of parameters that suppresses the fluctuation at the two-photon level does not suppress them at all N -photon levels, which means that the multi-photon emission cannot be precluded simultaneously at all orders. In other words,

the condition in Equation (15) that minimizes $g_s^{(2)}$, also minimizes the two-photon probability in the interference density matrix $\langle 2 | \rho_s | 2 \rangle$, at low intensities, but this is not the same condition that minimizes any other photon probability $\langle n | \rho_s | n \rangle$. This incompatibility is revealed by the n -norm, as defined in ref. [116], which is the distance in the correlation space between signal s and a perfect single-photon source.

$$\| (g_s^{(k)}) \|_n = \sqrt[n]{\sum_{k=2}^{n+1} [g_s^{(k)}]^n} \quad (18)$$

Figure 1c shows the 5-norm for the same range of parameters of Figure 1b. The dashed black line indicates the minimum values of $g_s^{(2)}$, which lies in a high-fluctuation region when the higher order correlation functions are taken into account. Further increasing n renders the correlation map completely red which means that multiphoton emission is not suppressed even if $g_s^{(2)}$ is close to zero. This is a feature typical of antibunching that arises from a two-photon interference only, that suggests that their use as single-photon sources may be an issue in the context of quantum technology where higher-photon correlations may jeopardize applications that rely on two-photon suppression. This is related to the fact that this antibunching stems from a Gaussian state, which is the most classical of the quantum states.

The decomposition of the second-order correlation as in Equation (6) is not limited to the particular case of interfering pure states set as initial conditions. This can also be applied to the dynamical case of a single system which provides itself and directly a coherent component α along with another, and therefore quantum, type of component. Calling s the annihilation operator for a particular emitter which has such a coherent—but not exclusively—component in its radiation, one can thus express its emission as the interference (or superposition) of a mean coherent field (s) and its quantum fluctuations, with operator $d = s - \langle s \rangle$. That is, one can always write

$$s = \langle s \rangle + d \quad (19)$$

Following the terminology introduced in the literature for a similar purpose,^[35] such an emission can be called self-homodyning. Since $g_s^{(2)}$ is also given by Equation (7) with the simplification brought by the fact that $\langle d \rangle = 0$, and by replacing $\alpha \rightarrow \langle s \rangle$ and $d \rightarrow s - \langle s \rangle$, general expressions in terms of $\langle s^{\dagger n} s^m \rangle$ for the emission of a single-emitter s , interfering its own components, is given by

$$\begin{aligned} \mathcal{I}_0 &= \frac{\left[\langle s^{\dagger 2} s^2 \rangle - \langle s^{\dagger} s \rangle^2 - 4|\langle s \rangle|^4 + 6|\langle s \rangle|^2 \langle s^{\dagger} s \rangle \right]}{\langle s^{\dagger} s \rangle^2} \\ \mathcal{I}_1 &= 4 \frac{\Re[\langle s^{\dagger} \rangle \langle s^{\dagger} s^2 \rangle - \langle s^{\dagger} \rangle^2 \langle s^2 \rangle] + 2|\langle s \rangle|^2 (|\langle s \rangle|^2 - \langle s^{\dagger} s \rangle)}{\langle s^{\dagger} s \rangle^2} \quad \text{and} \\ \mathcal{I}_2 &= 2 \frac{\Re[\langle s^{\dagger} \rangle^2 \langle s^2 \rangle] + |\langle s \rangle|^2 \langle s^{\dagger} s \rangle - 2|\langle s \rangle|^4}{\langle s^{\dagger} s \rangle^2} \quad (20) \end{aligned}$$

In the following sections, we will show how self-homodyning, Equations (20), explains by itself a huge amount of results scattered in the literature, that can be understood as interferences

between coherent and quantum components (that may or may not be of the squeezing type). This allows to better understand and analyze their statistical properties (anti- and superbunching) and contrast them with conventional blockade. We will focus on cases that are both fundamental and tightly related to each other, namely, the 2LS (resonance fluorescence in the Heitler regime) in Section 4, the anharmonic oscillator in Section 5, the Jaynes–Cummings Hamiltonian in Section 6 and microcavity polaritons in Section 7. Many systems in their low-driving regime are variations of these when not exact fits.

4. Heitler Regime of Resonance Fluorescence

We first consider the excitation of a two-level system (2LS) driven by a coherent source in the regime of low excitation—commonly referred to as the Heitler regime. Such a system is modeled by the Hamiltonian ($\hbar = 1$)

$$H_{\text{rf}} = (\omega_{\sigma} - \omega_{\text{L}}) \sigma^{\dagger} \sigma + \Omega_{\sigma} (\sigma^{\dagger} + \sigma) \quad (21)$$

This is the particular case of the general Hamiltonian (1) when only one mode is considered and $U \rightarrow \infty$. Here, the 2LS has a frequency ω_{σ} and is described with an annihilation operator σ that follows the pseudospin algebra, whereas the laser is treated classically, that is, as a complex number, with intensity Ω_{σ} (taken real without loss of generality) and frequency ω_{L} . The dynamics only depends on the frequency difference, $\Delta_{\sigma} \equiv \omega_{\sigma} - \omega_{\text{L}}$. The dissipative character of the system is included in the dynamics with a master equation $\partial_t \rho = i[\rho, H_{\text{rf}}] + (\gamma_{\sigma}/2) \mathcal{L}_{\sigma} \rho$ in the Lindblad form. The steady-state solution, computed by standard open quantum systems techniques,^[26] can be fully written in terms of two parameters: the 2LS population (or probability to be in the excited state) $\langle n_{\sigma} \rangle \equiv \langle \sigma^{\dagger} \sigma \rangle$, and the coherence or mean field $\alpha \equiv \langle \sigma \rangle$ ^[117]

$$\rho = \begin{pmatrix} 1 - \langle n_{\sigma} \rangle & \alpha^* \\ \alpha & \langle n_{\sigma} \rangle \end{pmatrix} \quad (22)$$

where

$$\langle n_{\sigma} \rangle = \frac{4\Omega_{\sigma}^2}{\gamma_{\sigma}^2 + 4\Delta_{\sigma}^2 + 8\Omega_{\sigma}^2} \quad \text{and} \quad \alpha = \frac{2\Omega_{\sigma}(2\Delta_{\sigma} + i\gamma_{\sigma})}{\gamma_{\sigma}^2 + 4\Delta_{\sigma}^2 + 8\Omega_{\sigma}^2} \quad (23)$$

As a consequence of the fermionic character of the 2LS, it can only sustain one excitation at a time. Therefore, all the correlators different from those in Equation (23) vanish, and in particular the N -photon correlations of the two-level system are exactly zero, namely $g_{\sigma}^{(N)} = 0$ for $N \geq 2$. We call this perfect cancellation of correlations to all orders conventional blockade or conventional antibunching (CA), as it arises from the natural Pauli blocking scenario. To investigate the components of the correlations that ultimately provide the perfect sub-Poissonian behavior of the signal, we separate the mean field from the fluctuations of the signal, $\sigma = \alpha + \epsilon$ in analogy with Equation (19). Following Equations (20), $g_{\sigma}^{(2)}$ can be decomposed as in Equation (6) with

$$\mathcal{I}_0 = \frac{|\alpha|^2 (6\langle n_{\sigma} \rangle - 4|\alpha|^2)}{n_{\sigma}^2} - 1 \quad (24a)$$

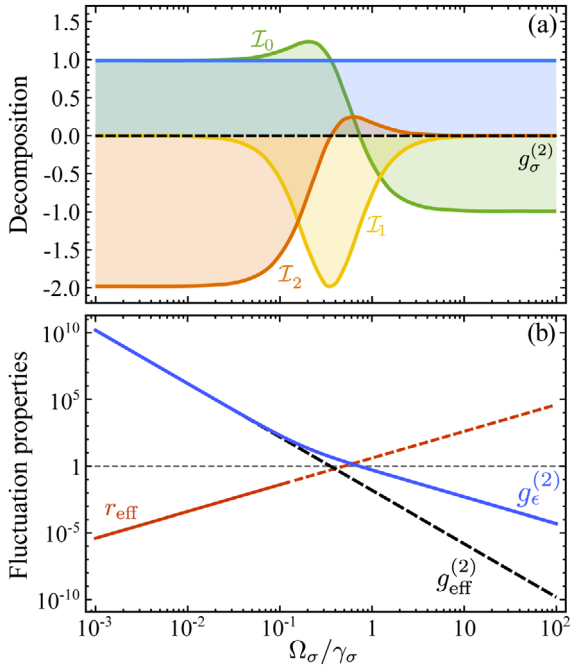


Figure 2. Second-order coherence function $g_{\sigma}^{(2)}$ (dashed black) of resonance fluorescence, as a function of the driving-laser intensity Ω_{σ} (at resonance). The Heitler regime, investigated in this work, is on the left ($\Omega_{\sigma} \ll \gamma_{\sigma}$). a) Decomposition of $g_{\sigma}^{(2)}$, given by Equation (20) with $s \rightarrow \sigma$, which cancels out to give an exact zero. b) Squeezing properties of the emitted light ($\Delta_{\sigma} = 0$), characterised by the effective squeezing parameter r_{eff} for the fluctuations only ϵ (red line), and statistics of the fluctuations $g_{\epsilon}^{(2)}$ (solid blue line), given by Equation (27). The latter can be approximated by $g_{\text{eff}}^{(2)}$ when the driving is low enough. The red solid line indicates when the effective squeezing parameter fits properly the actual statistics and becomes dashed when the approximation fails. In both cases, the range of validity is $\Omega_{\sigma} \lesssim 0.1\gamma_{\sigma}$.

$$I_1 = -8 \frac{|\alpha|^2 (\langle n_{\sigma} \rangle - |\alpha|^2)}{n_{\sigma}^2} \quad (24b)$$

$$I_2 = 2 \frac{|\alpha|^2 (\langle n_{\sigma} \rangle - 2|\alpha|^2)}{n_{\sigma}^2} \quad (24c)$$

These are presented in **Figure 2a** as a function of the intensity of the driving laser. The decomposition shows that, although the photon correlations of the 2LS are always perfectly sub-Poissonian, or antibunched, the nature of their cancellation varies depending on the driving regime.^[49] In the high-driving regime, the coherent component is compensated by the sub-Poissonian statistics of the quantum fluctuations ($I_0 < 0$) since $\lim_{\Omega_{\sigma} \rightarrow \infty} \alpha = 0$ and fluctuations become the total field, $\epsilon \rightarrow \sigma$. In contrast, in the Heitler regime the coherent component is compensated by the super-Poissonian but also squeezed fluctuations ($I_2 < 0$). The Heitler regime is, therefore, an example of the type of self-homodyne interference discussed in Section 3.

The fluctuations can be analyzed more closely through their correlation functions.

$$\langle \epsilon^{\dagger k} \epsilon^l \rangle = (-1)^{k+l} \alpha^{*k-1} \alpha^{l-1} (|\alpha|^2 (1 - k - l + kl) + kl \langle n_{\epsilon} \rangle) \quad (25)$$

where $\langle n_{\epsilon} \rangle = \langle n_{\sigma} \rangle - |\alpha|^2$ is the contribution from the fluctuations to the total population of the 2LS. The N -photon correlations from the fluctuations alone can be given in closed form [109]

$$g_{\epsilon}^{(N)} = \frac{|\alpha|^{2(N-1)} (N^2 \langle n_{\sigma} \rangle + (1 - 2N)|\alpha|^2)}{(\langle n_{\sigma} \rangle - |\alpha|^2)^N} \quad (26)$$

which, in terms of the physical parameters reads

$$g_{\epsilon}^{(N)} = \frac{(N-1)^2 (\gamma_{\sigma}^2 + 4\Delta_{\sigma}^2) + 8N^2 \Omega_{\sigma}^2}{8^N \Omega_{\sigma}^{2N} (\gamma_{\sigma}^2 + 4\Delta_{\sigma}^2)^{1-N}} \quad (27)$$

The two-photon fluctuation correlations $g_{\epsilon}^{(2)}$ are shown in **Figure 2b**, confirming that fluctuations are sub-Poissonian or super-Poissonian depending on whether the effective driving defined as $\Omega_{\text{eff}} \equiv \Omega_{\sigma} / \sqrt{1 + (2\Delta_{\sigma} / \gamma_{\sigma})^2}$ is much larger or smaller than the system decay γ_{σ} , respectively (the figure is for the resonant case).

In the Heitler regime, we need to consider only the magnitudes up to leading order in the effective normalized driving $p \equiv 2\Omega_{\text{eff}} / \gamma_{\sigma}$. The main contribution to the intensity $\langle n_{\sigma} \rangle = |\alpha|^2 + \langle n_{\epsilon} \rangle$, in the absence of pure dephasing, comes from the coherent part $|\alpha|^2$ of the signal. Fluctuations only appear to the next order, having, up to fourth order in p

$$\langle n_{\sigma} \rangle = p^2 - 2p^4, \quad |\alpha|^2 = p^2 - 4p^4 \quad \text{and} \quad \langle n_{\epsilon} \rangle = 2p^4 \quad (28)$$

The coherent contribution corresponds to the elastic (also known as ‘‘Rayleigh’’) scattering of the laser-photons by the two-level system, while the fluctuations originate from the two-photon excitation and re-emission.^[118] In the spectrum of emission, this manifests as a superposition of a delta and a Lorentzian peaks with exactly these weights, $|\alpha|^2$ and $\langle n_{\epsilon} \rangle$, both centered at the laser frequency, with no width (for an ideal laser) and γ_{σ} -width, respectively.^[49,119,120] Fluctuations have no coherent intensity by construction, $\langle \epsilon \rangle = 0$. At the same time, their second momentum is not zero but exactly the opposite of the coherent field one: $\langle \epsilon^2 \rangle = -\alpha^2$, thanks to the fact that $\langle \sigma^2 \rangle = \alpha^2 + \langle \epsilon^2 \rangle = 0$. This means that both contributions, coherent and incoherent, are of the same order in the driving p when it comes to two-photon processes and can, therefore, interfere and even cancel each other. This is precisely what happens and is made explicit in the $g_{\sigma}^{(2)}$ -decomposition above. The strong two-photon interference (I_2) can compensate the Poissonian and super-Poissonian statistics of the coherent and incoherent parts of the signal ($1 + I_0$). Since quadrature squeezing is created by a displacement operator, or a Hamiltonian, based on the operator ϵ^2 , this situation corresponds to a high degree of quadrature squeezing for the fluctuations. In fact, it can be shown^[109] that the incoherent population in the Heitler regime behaves to lowest order exactly like a squeezed thermal state with squeezing parameter $r_{\text{eff}} = 4\Omega_{\sigma}^2 / (\gamma_{\sigma}^2 + 4\Delta_{\sigma}^2)$ and effective thermal population $p_{\text{th}} \approx 16\Omega_{\sigma}^4 / (\gamma_{\sigma}^2 + 4\Delta_{\sigma}^2)^2$. From this, an effective $g^{(2)}$, namely $g_{\text{eff}}^{(2)}$, can be obtained for the fluctuations that also behave like a squeezed thermal state, for which correlations have been given above. Fixing $|\alpha| = 0$ in Equation (13b) and taking the limit $r_{\text{eff}}^2 \rightarrow 0$ and $p_{\text{th}} \rightarrow 0$ (both go to 0 with the

same power dependence), gives $g_{\text{eff}}^{(2)} \approx r_{\text{eff}}^2 / (r_{\text{eff}}^2 + p_{\text{th}})^2$ yielding, with substitution of the thermal parameters

$$g_{\text{eff}}^{(2)} \approx \frac{(\gamma_{\sigma}^2 + 4\Delta_{\sigma}^2)^2}{64\Omega_{\sigma}^4} \quad (29)$$

This is plotted in Figure 2b as a function of the driving, with the line becoming dashed when the interference can no longer be described in terms of a squeezed thermal state. Note that the total signal has no squeezing at low driving, only fluctuations do, because the coherent contribution is much larger.

Resonance fluorescence by itself always provides antibunching due to the perfect cancellation of the various components. However, one can disrupt this by manipulating the coherent fraction, simply by interfering the signal σ in a beam splitter with an external coherent state $|\beta\rangle$. This allows to change the photon statistics of the total signal $s = T\sigma + iR\beta$, where T^2 and R^2 are the transmittance and reflectance of the beam splitter. Actually, since the decomposition affects correlators to all orders, Equation (26), one can target the N -photon level instead of the two-photon one. Namely, one can decide to set the N -photon coherence function to zero. As a particular case, the 1-photon case cancels the signal altogether, which is obtained by solving the condition $\langle n_s \rangle = T^2|\alpha + iR\beta_1/T|^2 = 0$ (because $\langle n_{\sigma} \rangle = 0$ to second order in Ω_{σ}). We will show that the possibility to target one N in isolation of the others introduces a separate regime from conventional blockade. Given their relationship and in line with the terminology found in a large body of literature, we refer to this as unconventional blockade and unconventional antibunching (UA).

With this objective of tuning N -photon statistics and in order to avoid referencing the specificities of the beam splitter which do not change the normalized observables, let us define $\beta' \equiv R\beta/T \equiv |\beta'|e^{i\phi}$ and parameterize its amplitude as a fraction \mathcal{F} (always a positive number) of the laser field exciting the 2LS such that $|\beta'| = \Omega_{\sigma}\mathcal{F}/\gamma_{\sigma}$. This gives the coherence function $g_s^{(N)}$ of the interfered field in the Heitler regime as

$$g_s^{(N)} = \frac{T^{2N}}{\langle n_s \rangle^N} \frac{\mathcal{F}^{2(N-1)}\Omega_{\sigma}^{2N}}{\gamma_{\sigma}^{2N}(\gamma_{\sigma}^2 + 4\Delta_{\sigma}^2)} \left[\mathcal{F}^2(\gamma_{\sigma}^2 + 4\Delta_{\sigma}^2) + 4N\mathcal{F}\gamma_{\sigma}(\gamma_{\sigma}\cos\phi - 2\Delta_{\sigma}\sin\phi) + 4N^2\gamma_{\sigma}^2 \right] \quad (30)$$

One can appreciate the considerable enrichment brought by the interfering laser, by comparing $\langle n_s \rangle$ with the interfering laser, $\mathcal{F} \neq 0$, given by Equation (30) for $N = 1$ (since $g_s^{(1)} = 1$, this expression also provides the population) to the population $\langle n_{\sigma} \rangle$ without the laser, $\mathcal{F} = 0$, given by Equation (23), and even more so by comparing the N -photon correlation function, which is identically zero without the interfering laser, and that becomes Equation (30) with the interfering laser. Interestingly, there is now another condition that suppresses completely photon coincidences to yield a perfect antibunching at a given N -photon order, in addition to the one obtained in the original system without the interfering laser (CA). The new conditions exist for any detuning and are given by

$$\tan\phi_N = -\frac{2\Delta_{\sigma}}{\gamma_{\sigma}} \quad \text{and} \quad \mathcal{F}_N = -2N\cos\phi_N \quad (31)$$

Focusing on the resonance case for simplicity, we have $\mathcal{F}_N = 2N$ and always the same phase, $\phi_N = \pi$, which corresponds to the field $i\beta'_N = -N|\alpha|$. The total coherent fraction changes phase for all N : $\alpha + i\beta'_N = -(N-1)\alpha$. The signal population ($\langle n_s \rangle = G_s^{(1)}$) vanishes due to a first-order (or one-photon) interference at the external laser parameter $\mathcal{F}_1 = 2$, which translates into $i\beta'_1 = -i|\alpha|$. The external laser completely compensates the coherent fraction of resonance fluorescence, in this case $\alpha = i|\alpha|$ (with $|\alpha| = 2\Omega_{\sigma}/\gamma_{\sigma}$). This situation corresponds to a classical destructive interference, which equally occurs between two fully classical laser beams with the same intensity and opposite phase.

In the case of highest interest, that of two-photon correlations $g_s^{(2)}$, we find a destructive two-photon interference at the intensity $\mathcal{F}_2 = 4$, which corresponds to an external laser $i\beta'_2 = -2|\alpha|$, that fully inverts the sign of the coherent fraction in the total signal: $\alpha + i\beta'_2 = -\alpha$. This coherent contribution leads to perfect cancellation of the two-photon probability in the so-called wavefunction approach.^[121] Note that this does not, however, satisfy all other N -photon interference conditions and $g_s^{(N)}$ with $N > 2$ do not vanish. This is a very different situation as compared to the original resonance fluorescence where $g_{\sigma}^{(N)} = 0$ for all $N > 1$. One, the conventional scenario, arises from an interference that takes place at all orders. The other, the unconventional scenario, results from an interference that is specific to a given number of photons.

All these interferences, can be seen in Figure 3a up to $N = 4$. When there is no interference with the external laser, $\mathcal{F} = 0$, antibunching is perfect to all orders recovering resonance fluorescence. At the one-photon interference, the denominator of $g_s^{(N)}$ becomes zero and the functions, therefore, diverge. This produces a superbunching effect of a classical origin, as previously discussed: a destructive interference effect that brings the total intensity to zero. In this case, the external laser removes completely by destructive interference the coherent fraction of the total signal. Therefore, the statistics is that of the fluctuations alone, what we previously called $g_{\sigma}^{(N)}$, given by Equation (26). Note that the effect is also intrinsically difficult to measure as it is associated to a collapse of the signal. We have already discussed how, in the Heitler regime, fluctuations become super chaotic and squeezed. We can see, on the left hand side of Figure 1, that in the limit of $\Omega_{\sigma} \rightarrow 0$, they actually diverge. Such a superbunching is linked to noise. The resulting state is missing the one-photon component and, consequently, the next (dominating) component is the two-photon one. Nevertheless, there is not a suppression mechanism for components with higher number of photons so that the relevance of such a configuration for multiphoton (bundle) emission, remains to be investigated. We call this feature unconventional bunching (UB) in contrast with bunching that results from a N -photon de-excitation process that excludes explicitly the emission of other photon-numbers. This superbunching, as well as the antibunching by destructive interferences, will be reappearing in all the next systems of study. The Heitler regime is, therefore, a simple but rich system where all the squeezing-originated interferences already occur although we need an external laser to have them manifest.

We now return to the subtle point of which quantum state is realized by the various scenarios. To lowest-order in the driving, the dynamical state of the system can be described by a

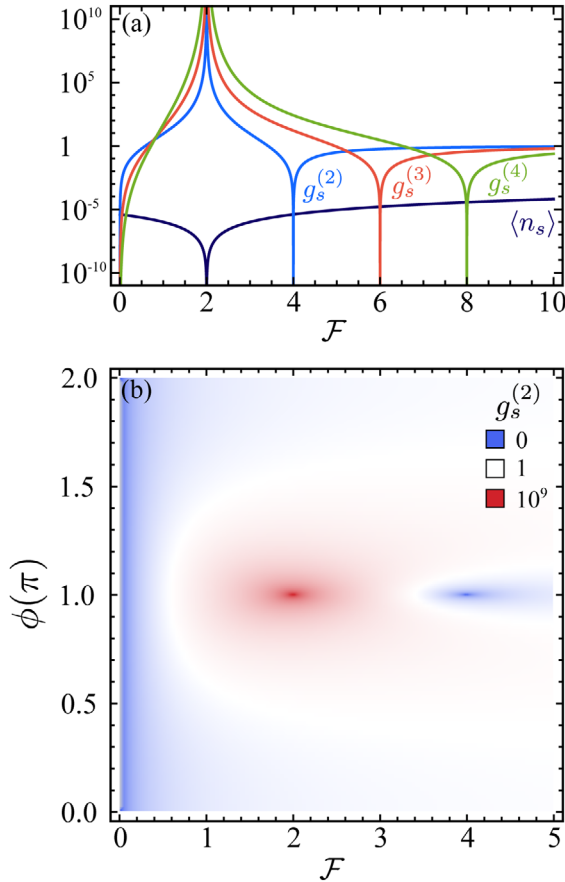


Figure 3. Interference between the output of resonance fluorescence and an external laser of intensity proportional to \mathcal{F} and phase ϕ . All modes at resonance. a) Intensity $\langle n_s \rangle$ and N -th order coherence functions $g_s^{(N)}$ of the resulting light as a function of \mathcal{F} . b) $g_s^{(2)}$ as a function of both \mathcal{F} and ϕ (in units of π) with the colour code in inset (log-scale). Tuning the external laser allows to choose between various resonant conditions.

superposition of a coherent and a squeezed state, insofar as only the lower-order correlation functions (namely, population and $g^{(2)}$) are considered. This is shown in Table 1, where we compare $g^{(N)}$ for $1 \leq N \leq 3$ (with $N = 1$ corresponding to the population) for the fluctuations in the Heitler regime versus the corresponding observables for a squeezed thermal state, on the one hand, and the laser-corrected configuration versus the displaced squeezed thermal state on the other hand. Such a

comparison is made by identifying the squeezing parameter and thermal populations to various orders in a series expansion of the quantum states with the corresponding observables from the dynamical systems, starting with r_{eff} and p_{th} introduced above. By definition, fluctuations have a vanishing mean, that is, $\langle \epsilon \rangle = 0$ so we must choose $\alpha = 0$. On the other hand, for the corrected emission, since one is blocking the two-photon contribution (at first order, this gives $g^{(2)} = 0$), the comparison with a displaced thermal state is obtained by imposing the condition for $g^{(2)}$ to vanish at first order ($r = |\alpha|^2$ and $\theta = 2\phi$). The results are compiled in the table up to the order at which they differ. Through the typical observables, namely, the population and $g^{(2)}$, one can see how the system is indeed well described to lowest order in the driving by a coherent squeezed thermal state (displaced if there is a laser-correction). However to next order, there is a departure, showing that the Gaussian state representation is an approximation valid up to second-order only. In fact, for three-photon correlations, the disagreement occurs already at the lowest-order in the driving, and is of a qualitative character, as is also shown in the table. Therefore, such a description is handy but breaks down if a high-enough number of photons or a too high-pumping is considered. What are the consequences of this for quantum applications of such states has not yet been settled in the literature.

5. Anharmonic Blockade

To show that the effects of conventional (self-homodyne interference at all N) and unconventional (self-homodyne interference at a given N only) blockades take place in a general setting and are not specific of strong quantum nonlinearities (such as a 2LS), we now address the case of a single anharmonic oscillator, that describes an interacting bosonic mode with a Kerr-type nonlinearity, which can be very weak. With driving by a coherent source (a laser) at frequency ω_L , its Hamiltonian reads

$$H_{\text{ao}} = \Delta_b b^\dagger b + \frac{U}{2} b^\dagger b^\dagger b b + \Omega_b (b^\dagger + b) \tag{32}$$

where the cavity operators are represented by b^\dagger and b , $\Delta_b = \omega_b - \omega_L$ is the detuning between the cavity and the laser, U denotes the particle interaction strength (that provides the nonlinearity) and the driving amplitude is given by Ω_b . This is the particular case of the general Hamiltonian (1) when only one mode is considered and U remains finite and, generally, small. The level structure of this system (at vanishing driving) is given by

Table 1. Two-level system. Comparison of first- (population), second- and third-order photon correlations, i) between a squeezed thermal state and the fluctuations in the Heitler regime and ii) between a displaced squeezed thermal state and the fluctuations in the laser-corrected Heitler regime, to various orders in the driving Ω_σ .

$g^{(N)}$	Squeezed thermal	Heitler fluctuations	Displaced squeezed thermal	Laser-corrected configuration
n_a	$\frac{32\Omega_\sigma^4}{\Gamma_\sigma^4} + \frac{1792\Omega_\sigma^8}{3\Gamma_\sigma^8} + O(\Omega_\sigma^{12})$	$\frac{32\Omega_\sigma^4}{\Gamma_\sigma^4} - \frac{512\Omega_\sigma^6}{\Gamma_\sigma^6} + O(\Omega_\sigma^8)$	$\frac{4\Omega_\sigma^2}{\Gamma_\sigma^2} + \frac{32\Omega_\sigma^4}{\Gamma_\sigma^4} + O(\Omega_\sigma^6)$	$\frac{4\Omega_\sigma^2}{\Gamma_\sigma^2} - \frac{32\Omega_\sigma^4}{\Gamma_\sigma^4} + O(\Omega_\sigma^6)$
$g^{(2)}$	$\frac{\Gamma_\sigma^4}{64\Omega_\sigma^4} + \frac{11}{4} + O(\Omega_\sigma^4)$	$\frac{\Gamma_\sigma^4}{64\Omega_\sigma^4} + \frac{\Gamma_\sigma^2}{2\Omega_\sigma^2} + O(\Omega_\sigma^0)$	$0 + \frac{32\Omega_\sigma^2}{\Gamma_\sigma^2} + O(\Omega_\sigma^4)$	$0 + \frac{128\Omega_\sigma^2}{\Gamma_\sigma^2} + O(\Omega_\sigma^4)$
$g^{(3)}$	$\frac{9\Gamma_\sigma^4}{64\Omega_\sigma^4} + \frac{51}{4} + O(\Omega_\sigma^4)$	$4 - \frac{96\Omega_\sigma^2}{\Gamma_\sigma^2} + O(\Omega_\sigma^4)$	$16 + \frac{768\Omega_\sigma^2}{\Gamma_\sigma^2} + O(\Omega_\sigma^4)$	$\frac{\Gamma_\sigma^6}{128\Omega_\sigma^6} + \frac{9\Gamma_\sigma^4}{64\Omega_\sigma^4} + O(\Omega_\sigma^{-2})$

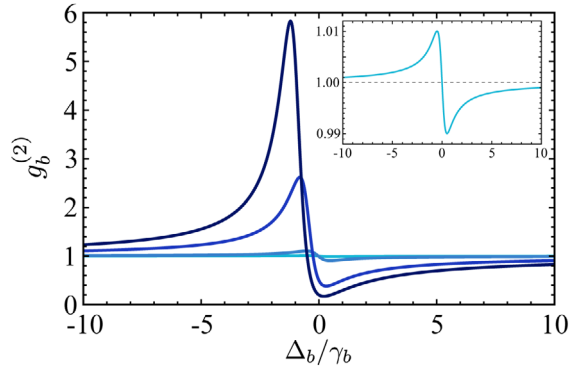


Figure 4. Second-order coherence function $g_b^{(2)}$ of an anharmonic oscillator, as a function of the detuning Δ_b . From light to dark blue, U increases (the exact values are $U/\gamma_b = 0.01, 0.1, 1, 2$, for fixed $\gamma_b = 1$). A zoom-in of the smallest case is shown in the inset.

the simple expression $E^{(N)} = N\omega_b + N(N-1)U$. The condition for the laser frequency to hit resonantly the N -photon level is $\omega_L = E^{(N)}/N$ (or $\Delta_b = -(N-1)U/2$).

We restrict our analysis of the dynamics $\dot{\rho} = -i[H_{\text{ao}}, \rho] + (\gamma_b/2)\mathcal{L}_b\rho$, with γ_b the decay rate of the mode, to the case of vanishing pumping, that is, $\Omega_b \ll \gamma_b$. Solving the correlator equations in this limit gives the population

$$\langle n_b \rangle = \frac{\Omega_b^2}{\gamma_b^2 + 4\Delta_b^2} \quad (33)$$

the second-order Glauber correlator

$$g_b^{(2)} = \frac{\langle b^\dagger b^\dagger bb \rangle}{\langle b^\dagger b \rangle^2} = \frac{(\gamma_b^2 + 4\Delta_b^2)}{\gamma_b^2 + (U + 2\Delta_b)^2} \quad (34)$$

as well as the higher-order correlators

$$g_b^{(N)} = \frac{(\gamma_b^2 + 4\Delta_b^2)^{N-1}}{\prod_{k=1}^{N-1} [\gamma_b^2 + (kU + 2\Delta_b)^2]} \quad (35)$$

This shows that, when scanning in frequency, $g_b^{(2)}$ has two extrema, one minimum and one maximum, as can be seen in **Figure 4**, whose positions are given by

$$\Delta_{\pm} = -\frac{1}{4} \left(U \pm \sqrt{U^2 + 4\gamma_b^2} \right) \quad (36)$$

with respective optimum antibunching (−) and bunching (+)

$$g_b^{(2)}(\Delta_b = \Delta_{\pm}) = 1 + \frac{U(U \pm \sqrt{U^2 + 4\gamma_b^2})}{2\gamma_b^2} \quad (37)$$

Both of these features are linked to the level structure: the antibunching condition is that of resonantly driving the first rung, $E^{(1)}$ (note that $\Delta_- \approx 0$, especially when $U \gg \gamma_b$), and the bunching condition, that of driving the second rung, $E^{(2)}$ ($\Delta_+ \approx -U/2$). In both cases, all other rungs are off-resonance and will remain much less occupied. Therefore, these effects are of a conventional

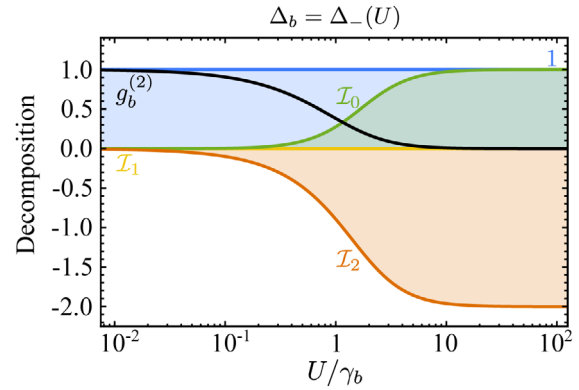


Figure 5. Second-order coherence function $g_b^{(2)}$ together with its decomposition, as a function of the non-linear interaction strength U following the conventional antibunching frequency $\Delta_b = \Delta_-(U)$.

nature, as we have defined it in the previous section: CA and conventional bunching (CB), respectively. The difference with resonance fluorescence is that here, CA is not a perfect interference at all orders ($g^{(N)} = 0$ for $N > 1$) but an approximated one. For instance, $g_b^{(2)}(\Delta_-) \approx (\gamma_b/U)^2$ (to leading order in U/γ_b), is only zero in the limit $U \rightarrow \infty$, when the system converges to a 2LS. On the other hand, there was not CB in resonance fluorescence due to the lack of levels $N > 1$. Here, we see it appearing for the first time.

The decomposition of $g_b^{(2)}$ according to Equation (6) yields

$$I_0 = \frac{U^2}{\gamma_b^2 + (U + 2\Delta_b)^2} \quad \text{and} \quad I_2 = -\frac{2U(U + 2\Delta_b)}{\gamma_b^2 + (U + 2\Delta_b)^2} \quad (38)$$

with $I_1 = 0$ in the limit of low driving (as in the case of the Heitler regime), which means that there are no anomalous correlations to leading order in Ω_b . $I_0 > 0$ means that fluctuations are always super-Poissonian. The remaining term I_2 can take positive (for $\Delta_b > -U/2$) and negative (for $\Delta_b < -U/2$) values, resulting in super-Poissonian statistics or, on the contrary, favouring antibunching. The various terms and the total $g_b^{(2)}$ are shown in **Figure 5** as a function of U , for the case $\Delta_b = \Delta_-(U)$ that maximizes antibunching, showing the evolution from Poissonian fluctuations in the linear regime of a driven harmonic mode to antibunching as the two-level limit is recovered with $I_0 \rightarrow 1$ and $I_2 \rightarrow -2$ (cf. Figure 2a).

As previously, the statistics can be modified by adjusting the coherent component of the original signal b with an external laser $\beta = |\beta|e^{i\phi}$. The resulting signal is then described by the operator $s = Tb + iR\beta$, with coherent contribution now given by $\langle s \rangle = T\langle b \rangle + iR\beta$. To simplify further the calculations, we choose $\beta = \frac{T}{R}\beta'$, where β' is also written in terms of the driving amplitude and an adimensional amplitude \mathcal{F}

$$\beta' = \frac{\Omega_b}{\gamma_b} \mathcal{F} \quad (39)$$

Additionally, we shift the phase $\phi \rightarrow \phi + \pi$, so in the limit of high U , all the results are consistent with the previous case. Then, the

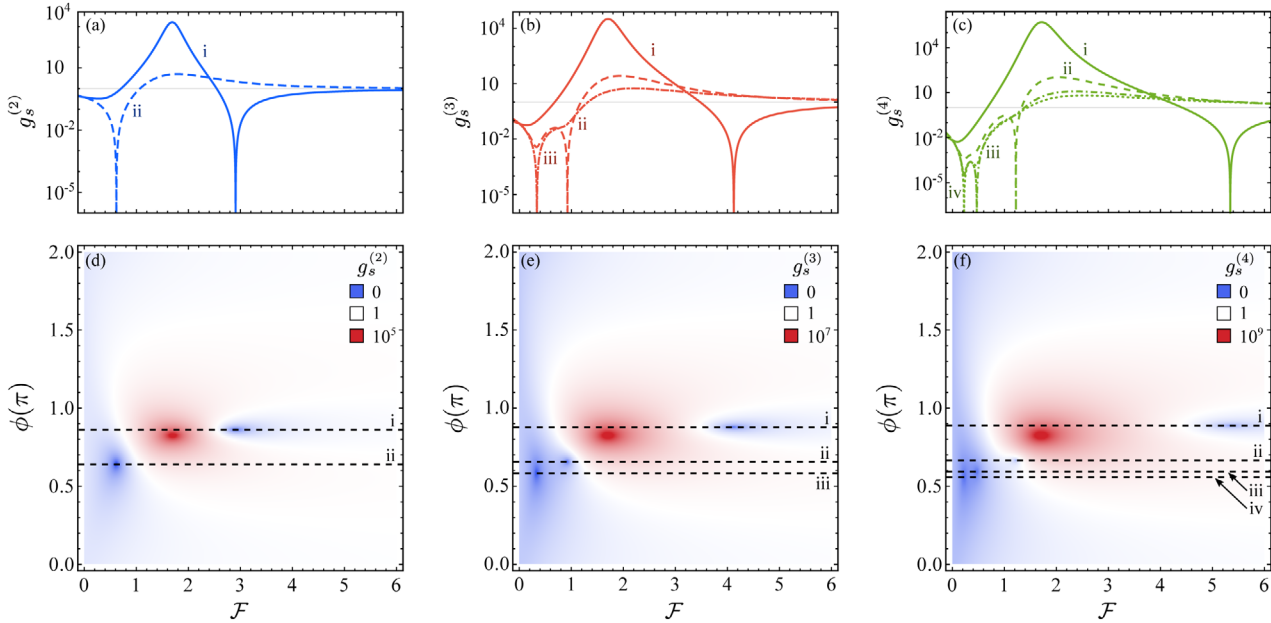


Figure 6. Interference between the output of a driven anharmonic system and an external laser of intensity proportional to \mathcal{F} and phase ϕ . Various columns shown increasing orders of photon correlations, with the upper row showing a phase-cut along the lines that intercept one of the resonances in the full landscape shown in the bottom row (the superbunching case is not shown). Parameters: $U = \gamma_b$, $\Omega_b = 0.001 \gamma_b$, $T^2 = 0.5$ and $\gamma_b = 1$.

total population becomes

$$\langle n_s \rangle = \frac{T^2 \Omega_b^2}{\gamma_b^2 (\gamma_b^2 + 4\Delta_b^2)} \left[\mathcal{F}^2 (\gamma_b^2 + 4\Delta_b^2) + 4\gamma_b \mathcal{F} (\gamma_b \cos \phi - 2\Delta_b \sin \phi) + 4\gamma_b^2 \right] \quad (40)$$

and the two-photon correlations become

$$\begin{aligned} g_s^{(2)} = & \bar{\Gamma}_b^2 \left\{ \bar{\Gamma}_b^2 [\gamma_b^2 + (U + \Delta_b)^2] \mathcal{F}^4 \right. \\ & - 8\gamma_b [\gamma_b^2 + (U + \Delta_b)^2] (\gamma_b \cos \phi - 2\Delta_b \sin \phi) \mathcal{F}^3 \\ & + [16\gamma_b^2 (\gamma_b^2 + (U + 2\Delta_b)^2) + 8\gamma_b^2 \cos 2\phi (\gamma_b^2 - 2\Delta_b (U + 2\Delta_b))] \\ & - 8\gamma_b^3 \sin 2\phi (U + 4\Delta_b) \mathcal{F}^2 \\ & \left. - 32\gamma_b^3 [\gamma_b \cos \phi - (U + 2\Delta_b) \sin \phi] \mathcal{F} + 16\gamma_b^4 \right\} / \\ & \left\{ [\gamma_b^2 + (U + 2\Delta_b)^2] \right. \\ & \left. \times [\mathcal{F}^2 (\gamma_b^2 + 4\Delta_b^2) + 4\gamma_b \mathcal{F} (\gamma_b \cos \phi - 2\Delta_b \sin \phi) + 4\gamma_b^2]^2 \right\} \quad (41) \end{aligned}$$

where we have used $\bar{\Gamma}_b^2 = \gamma_b^2 + 4\Delta_b^2$. Here as well, we can compare the enrichment brought by the interfering laser by comparing Equations (33) and (40) for populations and Equations (34) and (41) for second-order correlations, with and without the interference, respectively. In this case, higher-order correlators could also be given in closed-form but are too awkward to be written here. The cases $g_s^{(k)}$ for $2 \leq k \leq 4$ are shown in **Figure 6** as a function

of the parameters of the interfering laser. By comparing this to Figure 3 for the 2LS, one can see that the anharmonic system is significantly more complex, with resonances for the correlations that occur for specific conditions of the phase for each \mathcal{F} that leads to unconventional forms of antibunching or superbunching, rather than to be simply out-of-phase previously. This makes salient the punctual character of the unconventional mechanism: each strong correlation at any given order must be realized in a very particular way: the one that matches the corresponding interference.

The maximum bunching (UB) accessible with the interfering laser is reached when the coherent-fraction population goes to zero (1-photon suppression) for which the conditions on the phase and amplitude read $\tan \phi_1 = -2\Delta_b/\gamma_b$ and $\mathcal{F}_1 = -2 \cos \phi_1$. Those conditions are exactly the same as Equation (31) for $N = 1$. Analogous conditions for the multi-photon cases can be found solving $g_s^{(N)} = 0$. For the case $N = 2$, we find four different roots:

$$\mathcal{F}_{2,k} = \frac{2ie^{i\nu_k \phi} \gamma_b}{(U + 2\Delta_b) + i\nu_k \gamma_b} \left\{ 1 + \mu_k \sqrt{\frac{U}{(U + 2\Delta_b) + i\nu_k \gamma_b}} \right\} \quad (42)$$

with $k = 1, 2, 3, 4$ and $\nu_k = (-1)^{\lfloor k/3 \rfloor}$, $\mu_k = (-1)^{k+1}$ introduced to shorten the notations. Since these should be, by definition, real, this imposes another constrain on ϕ . Although the expression for real-valued ϕ to make \mathcal{F} real cannot be given in closed form, they are readily found numerically. It is possible to get four real solutions, that are however degenerate. There are only two different conditions for ϕ since the real part is the same for each pair of roots, that is, $\Re(\mathcal{F}_{2,1}) = \Re(\mathcal{F}_{2,4})$ and $\Re(\mathcal{F}_{2,2}) = \Re(\mathcal{F}_{2,3})$. This yields two physical solutions. For instance, for $U = \gamma_b$ and $\Delta_b = \Delta_-$ (the case shown in Figure 6), $g_s^{(2)}$ vanishes at $\mathcal{F}_{2,1} \approx 0.615$ and $\phi_{2,1} \approx 0.659 \pi$ for one solution and at $\mathcal{F}_{2,2} \approx 2.907$ and $\phi_{2,2} \approx 0.860 \pi$

Table 2. Anharmonic oscillator. Comparison of first- (population), second-, and third-order photon correlations, i) between a displaced squeezed thermal state and the anharmonic oscillator with $\Delta_b = \Delta_-$ (optimal antibunching) and ii) between a displaced squeezed thermal state and the laser-corrected for the optimal $g^{(2)}$ configuration ($F_{2,2}$ and $\phi_{2,2}$). The abbreviated notation $\tilde{\Omega}_b$ indicates the normalized pumping referred to the cavity decay, that is, $\tilde{\Omega}_b/\gamma_b$. We have also taken $\gamma_b = U$ for concision of the expressions.

$g^{(N)}$	Displaced squeezed thermal	AO antibunching	Displaced squeezed thermal	Laser-corrected configuration
n_a	$2.89\tilde{\Omega}_b^2 + 4.63\tilde{\Omega}_b^4 + O(\tilde{\Omega}_b^6)$	$2.89\tilde{\Omega}_b^2 - 10.36\tilde{\Omega}_b^4 + O(\tilde{\Omega}_b^6)$	$1.52\tilde{\Omega}_b^2 + 4.63\tilde{\Omega}_b^4 + O(\tilde{\Omega}_b^6)$	$1.52\tilde{\Omega}_b^2 - 3.25\tilde{\Omega}_b^4 + O(\tilde{\Omega}_b^6)$
$g^{(2)}$	$0.38 + 5.18\tilde{\Omega}_b^2 + O(\tilde{\Omega}_b^4)$	$0.38 + 0.91\tilde{\Omega}_b^2 + O(\tilde{\Omega}_b^4)$	$0 + 12.75\tilde{\Omega}_b^2 + O(\tilde{\Omega}_b^4)$	$0 + 47.84\tilde{\Omega}_b^2 + O(\tilde{\Omega}_b^4)$
$g^{(3)}$	$0.80 + 1.64\tilde{\Omega}_b^2 + O(\tilde{\Omega}_b^4)$	$0.06 + 0.37\tilde{\Omega}_b^2 + O(\tilde{\Omega}_b^4)$	$4 - 34.52\tilde{\Omega}_b^2 + O(\tilde{\Omega}_b^4)$	$0.71 + 0.78\tilde{\Omega}_b^2 + O(\tilde{\Omega}_b^4)$

for the other one. Similar resonances in higher-order correlations could be found following the same procedure.

Regarding the quantum state realized in the system, similar conclusions can be drawn for the anharmonic oscillator than for the two-level system (previous section, cf. Tables 1 and 2). Specifically for this case, the system can be described by a displaced squeezed thermal state, properly parameterized, but to lowest-order in the driving and for the population and the two-photon correlation only. Departures arise to next-order in the pumping or to any-order for three-photon correlations and higher. The main differences is that the anharmonic oscillator case has to be worked out numerically, so the prefactors are given by the solutions that optimize the antibunching, for the system parameters indicated in the caption. The same result otherwise holds that the Gaussian-state description is a low-driving approximation valid for the population and two-photon statistics. We find this again for the systems studied in the following sections, although this point will not be stressed anymore.

6. Jaynes–Cummings Blockade

Now that we have considered the two-level system on the one hand (Section 4) and the bosonic mode on the other hand (Section 5), we turn to the richer and intricate physics of their coupling. We will show how the themes of the previous sections allow us to unify in a fairly concise picture the great variety of phenomena observed and/or reported in isolation. We thus consider the case where a cavity mode, with bosonic annihilation operator a and frequency ω_a is coupled with strength g to a 2LS, with operator σ and frequency ω_σ , as described by the Jaynes–Cummings Hamiltonian.^[122,123]

$$H_{\text{JC}} = \Delta_\sigma \sigma^\dagger \sigma + \Delta_a a^\dagger a + g(a^\dagger \sigma + \sigma^\dagger a) + \Omega_a (e^{i\phi} a^\dagger + e^{-i\phi} a) + \Omega_\sigma (\sigma^\dagger + \sigma) \quad (43)$$

with $\Delta_\sigma \equiv \omega_\sigma - \omega_L$ and $\Delta_a \equiv \omega_a - \omega_L$ the detunings from the laser, and where we also include both a cavity and a 2LS driving term by a laser of frequency ω_L , with respective intensities Ω_a and Ω_σ and relative phase ϕ . We assume g and Ω_σ to be real numbers, without loss of generality since the magnitudes of interest ($G_a^{(N)}$) are independent of their phases. The relative phase ϕ between dot and cavity drivings is, on the other hand, important. We also limit ourselves in this text to the case where the frequencies of the dot and cavity drivings ω_L are identical and the analysis could be pushed further to the case where this limi-

tation is lifted. The dissipation is taken into account through the master equation $\partial_t \rho = i[\rho, H_{\text{JC}}] + (\gamma_\sigma/2)\mathcal{L}_\sigma \rho + (\gamma_a/2)\mathcal{L}_a \rho$ where γ_a is the decay rate of the cavity. Solving for the steady state in the low-driving regime, that is, when $\Omega_a \ll \gamma_a, \gamma_\sigma$, yields for the populations,^[109]

$$\langle n_a \rangle = 4 \frac{4g^2\Omega_a^2 + \tilde{\Gamma}_\sigma^2\Omega_a^2 - 4g\Omega_a\Omega_\sigma (\pm 2\Delta_\sigma \cos \phi + \gamma_\sigma \sin \phi)}{16g^4 + 8g^2(\gamma_a\gamma_\sigma - 4\Delta_a\Delta_\sigma) + \tilde{\Gamma}_\sigma^2\tilde{\Gamma}_\sigma^2} \quad (44)$$

with matching upper/lower indices (including \pm) and with $\tilde{\Gamma}_i^2 = \gamma_i^2 + 4\Delta_i^2$ (for $i = a, \sigma$). Similarly, the two-photon coherence function from the cavity can be found as follows:

$$g_a^{(2)} = \left\{ [16g^4 + 8g^2(\gamma_a\gamma_\sigma - 4\Delta_a\Delta_\sigma) + \tilde{\Gamma}_\sigma^2\tilde{\Gamma}_\sigma^2] \times [16g^4(1 + \chi^2) + 8g^2(2\chi^2\tilde{\Gamma}_{11}^2 + 4\Delta_\sigma\tilde{\Delta}_{11} - \gamma_\sigma\tilde{\gamma}_{11}) + \tilde{\Gamma}_\sigma^2\tilde{\Gamma}_{11}^2 - 16g\chi(\Delta_\sigma\tilde{\Gamma}_{11}^2 + 4g^2\tilde{\Delta}_{11}[1 + \chi^2]) \cos \phi + 8g^2\chi^2(4g^2 - \gamma_\sigma\tilde{\gamma}_{11} + 4\Delta_\sigma\tilde{\Delta}_{11}) \cos 2\phi - 8g\chi(\gamma_\sigma\tilde{\Gamma}_{11}^2 + 4g^2\tilde{\gamma}_{11}[\chi^2 - 1]) \sin \phi + 16g^2\chi^2(\gamma_a\Delta_\sigma + \gamma_\sigma\tilde{\Delta}_{12}) \sin 2\phi] \right\} / \left\{ [16g^4 + 8g^2(\gamma_a\tilde{\gamma}_{11} - 4\Delta_a\tilde{\Delta}_{11}) + \tilde{\Gamma}_\sigma^2\tilde{\Gamma}_{11}^2] \times [4g^2\chi^2 + \tilde{\Gamma}_\sigma^2 - 4g\chi(2\Delta_\sigma \cos \phi + \gamma_\sigma \sin \phi)]^2 \right\} \quad (45)$$

where $\tilde{\Delta}_{ij} \equiv i\Delta_a + j\Delta_\sigma$, $\tilde{\gamma}_{ij} = i\gamma_a + j\gamma_\sigma$, $\tilde{\Gamma}_{ij}^2 \equiv \tilde{\gamma}_{ij}^2 + 4\tilde{\Delta}_{ij}^2$ and $\chi = \Omega_\sigma/\Omega_a$ is the ratio of excitation. The range of χ extends from 0 to ∞ so that it is convenient to use the derived quantity $\tilde{\chi} = \frac{2}{\pi} \text{atan}(\chi)$, which varies between 0 and 1. Equation (45) is admittedly not enlightening per se but it contains all the physics of conventional and unconventional photon statistics that arises from self-homodyning, including bunching and antibunching, for all the regimes of operations. It is remarkable that so much physics of dressed-state blockades and interferences can be packed-up so concisely.

We plot a particular case of this formula as a function of ω_a and ω_L in **Figure 7a**, namely, only driving the cavity ($\Omega_\sigma = \chi = 0$), in which case the expression halves in size.^[109] The general case is available through an applet^[124] and we will shortly discuss other cases as well. The structure that is thus revealed can be decomposed in two classes, as shown in **Figure 7b**: the conventional

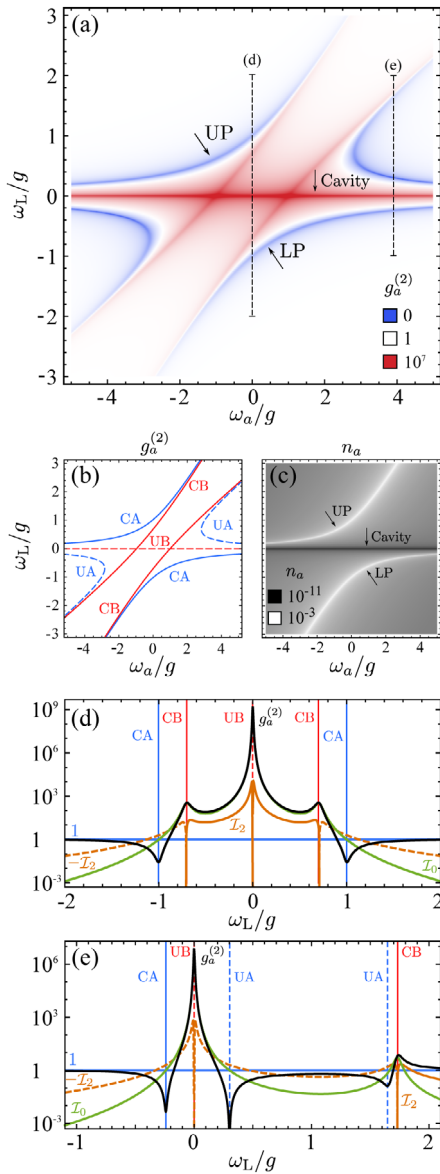


Figure 7. Jaynes–Cummings model. a) Photon statistics $g_a^{(2)}$ (log scale). b) Structure in terms of conventional C (solid) and unconventional U (dashed) features for B, bunching (red) and A, antibunching (blue). CA (CB) is given by the resonant condition with the first (second) JC rung (cf. Equations (46)). UA is given by the interference condition Equation (47) and UB by $\omega_L = 0$. c) Population n_a , showing that i) only polariton emit strongly and ii) how the depletion (not an exact zero) at $\omega_L = 0$ accounts for UB. Other features are not visible in the population only. d,e) $g_a^{(2)}$ (black line) for the two cuts shown in dashed lines in (a) with the cavity frequency either d) resonant with the 2LS or e) chosen to optimize UA ($\omega_a = 29.5\gamma_a$). The decomposition in I_j components is also shown, with the sign of I_2 changed when it is negative and plotted dashed. Parameters: $\omega_\sigma = 0$, $\gamma_a = 0.1g$, and $\gamma_\sigma = 0.01g$.

statistics that originates from the nonlinear properties of the quantum levels, in solid lines, and the unconventional statistics that originates from interferences, in dashed lines. Both can give rise to bunching (in red) and antibunching (in blue). We now discuss them in details.

6.1. Conventional Statistics

Conventional features arise from the laser entering in resonance with a dressed state of the dissipative JC ladder,^[125,126] which energy is the real part of

$$E_{\pm}^{(N)} = N\omega_a + \frac{\omega_\sigma - \omega_a}{2} - i\frac{(2N-1)\gamma_a + \gamma_\sigma}{4} \pm \sqrt{(\sqrt{N}g)^2 + \left(\frac{\omega_a - \omega_\sigma}{2} - i\frac{\gamma_a - \gamma_\sigma}{4}\right)^2} \quad (46)$$

The first rung $E_{\pm}^{(1)}$ yields the CA lines in Figure 7b. This corresponds to an increase in the cavity population, as shown in Figure 7c as two white lines, corresponding to the familiar lower and upper branches of strong coupling. This figure also makes clear how the signal is increased when hitting the first rung (Rabi doublet) and strongly suppressed at the UB condition. The system effectively gets excited, but through its first rung only. The second rung blocks further excitation according to the conventional antibunching (CA), or photon-blockade, scenario, so that with the increase of population goes a decrease of two-photon excitation, leading to antibunching. This is in complete analogy with the CA that appears in the Heitler regime of resonance fluorescence. This is not an exact zero in $g_a^{(2)}$ in the low driving regime (the imaginary part of the root does not vanish) because the conditions for perfect interference are no longer met having a strongly coupled cavity with a decay rate. It was recently shown^[49] that even in the vanishing coupling regime, $g \rightarrow 0$, when the cavity acts as a mere detector of the 2LS emission, perfect antibunching is reduced due to the finite decay rate (γ_a representing the precision in frequency detection). This is due to the fact that the cavity is effectively filtering out some of the incoherent fraction of the emission while the coherent fraction is still fully collected. The interference condition in the $g_a^{(2)}$ decomposition, $1 + I_1 = -I_2 = 2$, is no longer satisfied (see Figure 2 of ref. [49]).

On the other hand, driving resonantly the second rung, $E_{\pm}^{(2)}$, leads to conventional bunching (CB), shown as red solid lines in Figure 7b. These quantum features are well known and also found with incoherent driving of the system in the spectrum of emission^[126]; they are not conditional to the coherence of the driving. This also corresponds to an increase in the cavity population, although this is not showing in Figure 7c, where only first-order effects appear.

6.2. Unconventional Statistics

We now turn to the other features in $g_a^{(2)}$ that do not correspond to a resonant condition with a dressed state: these are, first, a superbunching line at $\omega_L = 0$ (dashed red in Figure 7b) and second, two symmetric antibunched lines (dashed blue). All correspond to a self-homodyne interference that the coherent field driving the cavity can produce on its own, without the need of a second external laser. In this case, this also involves several modes (degrees of freedom) and more parameters than in resonance fluorescence, so the phenomenology is richer, but can be tracked down to the same physics. We call them again unconventional

antibunching (UA) and unconventional bunching (UB) in full analogy with the Heitler regime of resonance fluorescence and in agreement with the literature that refers to particular cases of this phenomenology as “unconventional blockade”^[33] (the term “tunnelling” has also been employed but the underlying physical picture might be misleading^[10]).

We first address antibunching (UA). This is found by minimizing $g_a^{(2)}$ in regions where there is no CA, which yields (for the particular case $\chi = 0$)

$$\Delta_a = -\Delta_\sigma \left(1 + \frac{4g^2}{\gamma_\sigma^2 + 4\Delta_\sigma^2} \right) \quad (47)$$

which is the analytical expression for the the dashed blue lines in Figure 7b (we remind that $\Delta_i \equiv \omega_i - \omega_L$ for $i = a, \sigma$). The most general case when both the emitter and cavity are excited can be found in ref. [109]. The minimization process also provides the condition for CA, due to the first-rung resonance, but this can be disconnected from UA beyond the fact that CA is already identified because UA also admits an exact zero, which is found by either solving $g_a^{(2)} = 0$ or setting to zero the two-photon probability in the wavefunction approximation.^[121] This gives the conditions on the detunings as function of the system parameters^[127]

$$\Delta_\sigma^2 = \frac{\gamma_\sigma^2}{4} \left(\frac{4g^2}{\gamma_\sigma(\gamma_\sigma + \gamma_a)} - 1 \right) \quad (48a)$$

$$\Delta_a = - \left(2 + \frac{\gamma_a}{\gamma_\sigma} \right) \Delta_\sigma \quad (48b)$$

These conditions are met in Figure 7a at the lowest point where the blue UA line intersects the (e) cut (and on the symmetric point $\omega_a < 0$). When the laser is at resonance with the 2LS ($\Delta_\sigma = 0$) and cavity losses are large ($\gamma_a \gg \gamma_\sigma$), this occurs when the cooperativity $\mathcal{C} \equiv \frac{4g^2}{\gamma_a\gamma_\sigma} = 1$. This type of UA interference is second-order, so it is not apparent in the cavity population at low driving, Figure 7b. One has to turn to two-photon correlations instead. Note also that UA requires a cavity-emitter detuning that is of the order of g .

Since this is an interference effect, we perform the same decomposition of $g_a^{(2)}$ in terms of coherent and incoherent fractions, as in previous sections, given by Equation (6), and show the terms that are not zero in Figure 7d,e. The full expressions are given in ref. [109]. The term \mathcal{I}_1 is exactly zero to lowest order in the driving and only the fluctuation-statistics \mathcal{I}_0 and the two-photon interference \mathcal{I}_2 play a role, like in the Heitler regime of resonance fluorescence. Note that in this decomposition, there is no difference between the CA and UA, since both occur approximately when the statistics of the laser and fluctuations, $1 + \mathcal{I}_0 = 2$, are compensated by their two-photon interference, $\mathcal{I}_2 = -2$, again as in the Heitler regime. The fundamental differences between these two types of antibunching will be discussed later on. Before that, we address the last feature: the unconventional bunching at $\omega_L = 0$.

The reason for the super-bunching peak labeled as UB in Figure 7b is also the same as in resonance fluorescence: the cancellation of the coherent part, in this case, of the cavity emission, and the consequent dominance of the fluctuations only, which are super-Poissonian in this region. Therefore, contrary to the CB,

this superbunched statistics is not directly linked to an enhanced N -photon (for any N) emission and it does not appear one could harvest or Purcell-enhance it, for instance, by coupling the system to an auxiliary resonant cavity. Since it is pretty much wildly fluctuating noise, the actual prospects of multi-photon physics in this context remains to be investigated. In any case, the conditions that yield the super-Poissonian correlations can thus be obtained by minimizing the cavity population $\langle n_a \rangle$ or, from the wavefunction approach, by minimizing the probability to have one photon, which coincide with the coherent fraction to lowest order in Ω_a . One cannot achieve an exact zero in this case but the cavity population is clearly undergoing a destructive interference, as shown by the black horizontal line in Figure 7c. The resulting condition, $\Delta_\sigma = \chi g \cos \phi$, links the laser frequency with the 2LS one: which reduces to simply $\Delta_\sigma = 0$ (laser in resonance with the 2LS) if i) the dot and cavity are driven with a $\pi/2$ -phase difference or ii) the laser drives the cavity only ($\chi = 0$).

So far, we have focused on the particular case of Equation (45) where $\Omega_\sigma = 0$. This is the case dominantly studied in the literature and the one assumed to best reflect the experimental situation. It is also for our purpose a good choice to clarify the phenomenology that is taking place and how various types of statistics cohabit. It must be emphasized, however, that while the physics is essentially the same in the more general configuration, the results are, even qualitatively, significantly different in configurations where the two types of pumping are present. This is shown in Figure 8. While conventional features are stable, being pinned to the level structure, the unconventional ones that are due to interferences are very sensitive to the excitation conditions and get displaced or, in the case of QD excitation only, even completely suppressed. If one is to regard conventional features as more desirable for applications, this figure is therefore again an exhortation at focusing on the QD excitation configuration. Also, one can notice that CA and UA lines can meet when both types of pumping are present, as shown in Figure 8e,j. This is actually a valuable intersection that brings together the best of both mechanisms, namely, the low-antibunching of UA and the high-population and all-order suppression of CA.^[109]

While we have focused on the two-photon statistics, both the conventional and unconventional effects occur at the N -photon level, in which case they manifest through higher-order coherence functions $g^{(N)}$, and their N th-order behavior is one of the key differences between conventional and unconventional statistics. Regarding conventional features, resonances happen at the N -photon level when N photons of the laser have the same energy than one of the dressed states (and only one, thanks to the JC nonlinearities): $\omega_L = \text{Re}\{E_\pm^{(N)}\}/N$. The blockade that is realized is a real blockade in the sense that all the correlation functions are then depleted simultaneously. In Figure 9, the counterpart of Figure 7a is shown for $g_a^{(3)}$ and $g_a^{(4)}$ and shows how more conventional features appear with increasing N but otherwise stay pinned to the same conditions, while the number of unconventional features stays the same, but their positions drift with N , so that one cannot simultaneously realize $g_a^{(N)} < 1$ for all N . This is an important difference between a convex mixture of Gaussian states, which is a semi-classical state, and a state beyond this class, which is genuinely quantum, as previously mentioned. The latter requires the ability to imprint strong correlations at several

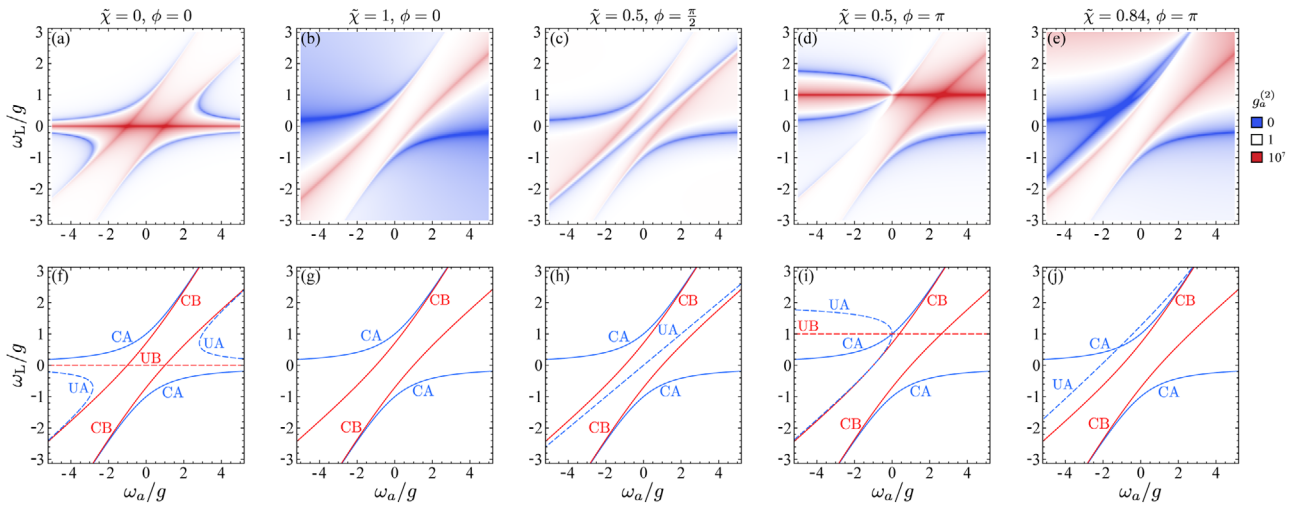


Figure 8. Effect of the type of driving on the two-photon statistics in the cavity emission of the Jaynes–Cummings model. The upper row shows Equation (45) for the parameters indicated in each panel and the lower row identifies the various features through the structure of conventional (Equation (46 c), solid) and unconventional (Equation (47), dashed) lines. Chosen parameters: $\gamma_a = 0.1 g$, $\gamma_\sigma = 0.01 g$.

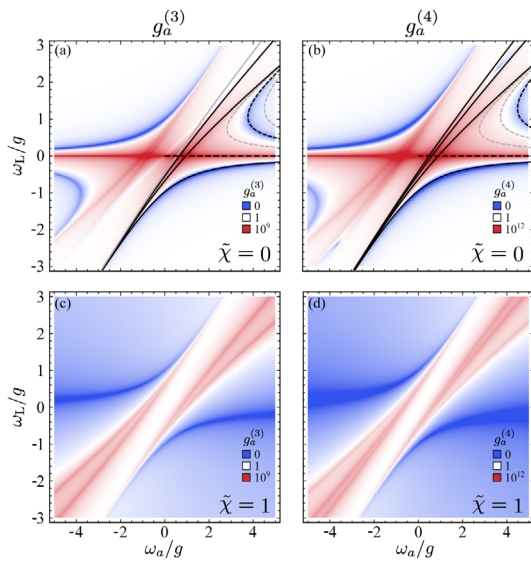


Figure 9. Higher-order photon statistics, at (left column) three- and (right) four-photon level. Top row is for cavity excitation and bottom row for 2LS excitation. In the top row, we have superimposed the right-half of the conventional (solid) and unconventional (dashed) features, putting them in grey when not present for a given order of the correlations. The conventional features grow in numbers and stay pinned at the same positions, while the unconventional ones remain in the same number but at different positions. Parameters: $\gamma_a = 0.1 g$, $\gamma_\sigma = 0.001 g$.

and possibly all photon-orders. This suggests that CA could be more suited than UA for quantum applications. Note how with the 2LS direct excitation, shown in the second row of Figure 9, one only finds conventional statistics, with magnified features such as broader antibunching in the photon-like branch and narrower one in the exciton-like branch. The N -photon resonances are neatly separated for large-enough detuning, which is the underlying principle to harness rich N -photon resources.^[128]

We now turn to another noteworthy regime, out of the many configurations of interest that are covered by Equation (45), namely, the transition from weak to strong coupling. The so-called strong-coupling, when $g > |\gamma_a - \gamma_\sigma|/4$, is one of the coveted attributes of light–matter interactions, leading to the emergence of dressed states and to a new realm of physics. It is also, however, an ill-defined concept in the presence of detuning^[126] and one would still find the dressed-state structure of Figure 9 in the largely detuned regime when driving the 2LS, even up to large photon-order.^[26] The restructuring of the statistics when crossing over to the weak-coupling regime is explored in Figure 10a, where we track the impact on $g_a^{(2)}$ of changing the coupling g , on the cut in Figure 7e that intersects from top to bottom CB, UA (twice), UB, and CA. One can see how the features converge as the coupling is reduced, with the conventional ones disappearing first, which is expected from the disappearance of the underlying dressed states that are responsible for the conventional effects. The unconventional antibunching, on the other hand, is more resilient and can be tracked well into weak coupling where all effects ultimately vanish at the same time as they merge. Conventional antibunching is the most robust feature, as can be seen by tracking, for instance, the UB peak at the point where it is the most isolated from the other features, namely, at resonance where $\omega_L = \omega_a = \omega_\sigma = 0$. Spanning over the two main parameters that control strong coupling, the coupling strength g (in units of γ_σ) and the rates of dissipation γ_a/γ_σ , one sees that the strong bunching is not always sustained but can be instead overtaken by conventional antibunching, which is the well-defined blue line in the figure (given by Equation (47)). The region where the UB peak is well-defined can be identified by inspecting the second derivative of $g_a^{(2)}$ as a function of the laser frequency, $\partial_{\omega_L}^2 g_a^{(2)}$ at $\omega_L = 0$ and is shown in Figure 10b as a dashed black line. The white line that separates the antibunching region from the bunching one corresponds to the critical coupling strength g_p between the cavity and the 2LS that leads to $g_a^{(2)} = 1$ (its expression is given in ref. [109]). The strong-weak coupling

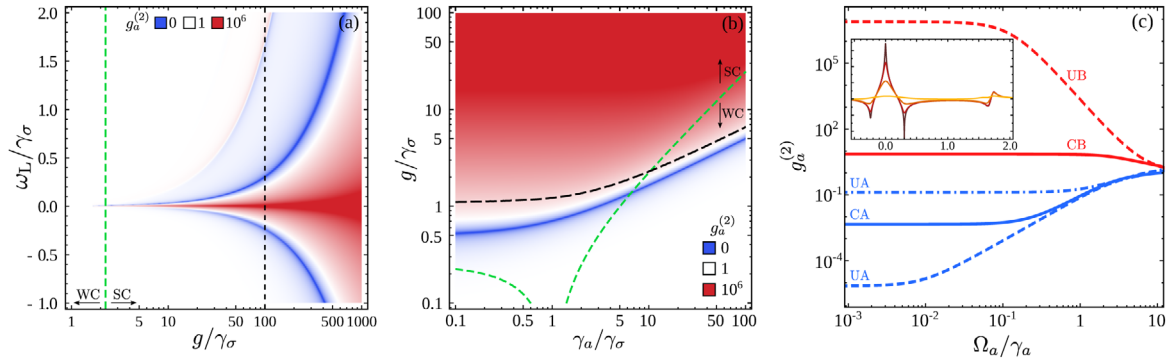


Figure 10. Transition to weak coupling and non-vanishing pumping. a) Evolution of $g_a^{(2)}$ along the cut (e) in Figure 7 as a function of the coupling strength g , showing how the structure collapses on the bare modes. CA (lowest blue line) is the first feature to vanish with decreasing g , as the underlying dressed states disappear. b) Behavior of the “center” point at $\omega_L = \omega_a = 0$ that typically features the UB peak, although not exclusively as it can also exhibit antibunching, even in strong-coupling (Black dashed line indicates when the behavior of $g_a^{(2)}$ changes from local minimum to maximum). c) Effect of increasing pumping, computing the features shown in Figure 7e) (vanishing pumping) as a function of (finite) driving Ω_a . For high pumping, $\Omega_a \gtrsim \gamma_a$, every feature (both bunching and antibunching) is spoiled and eventually disappears ($g_a^{(2)} \rightarrow 1$). The inset figure compares the same cut of $g_a^{(2)}$ for the cases of vanishing driving ($\Omega_a \rightarrow 0$) and finite driving ($\Omega_a/\gamma_a = 0.5, 2,$ and 10). Lighter colors correspond to higher driving amplitudes.

frontier $g/\gamma_\sigma < |\gamma_a/\gamma_\sigma - 1|/4$ is indicated with a dotted green line as a reference, illustrating again the lack of close connection between strong-coupling and the photon-statistics features.

We conclude the discussion of the Jaynes–Cummings system with the second main difference between conventional and unconventional statistics, namely their resilience to higher driving. All our results are exact in the limit of vanishing driving, that is to say, in the approximation of neglecting Ω terms of higher-orders than the smallest contributing one. For non-vanishing driving, numerically exact results can be obtained instead (and can be made to agree with arbitrary precision to the analytical expressions, as long as the driving is taken low enough, what we have consistently checked). A characteristic of the unconventional features is that, being due to an interference effect for a given photon number only, it is fragile to driving, unlike the conventional features which display more robustness. This is illustrated in Figure 10c for the case of cavity driving Ω_a , where we compare the analytical result from Equation (45), in black, with the numerical solution for $\Omega_a = 0.25\gamma_a$, so still fairly small. One can see how the conventional features are qualitatively preserved and quantitatively similar to the analytical result, while the unconventional antibunching has been completely washed out. One could consider still other aspects of the physics embedded in Equation (45), such as the adverse effect of increasing pumping to increase the signal. The inquisitive reader can explore them through the applet.^[124] Instead of discussing these further, we now turn to another platform of interest that bears many similarities with the Jaynes–Cummings results.

7. Polariton Blockade

Microcavity polaritons^[26] arise from the strong coupling (with coupling g) between a cavity photon a of frequency ω_a and a material excitation b of frequency ω_b , both assumed here to be bosonic fields. The material excitation exhibits an interaction of some sort (Coulomb interactions for excitons–polaritons since excitons are electron–hole pairs) that we parameterize as $U/2$. Thus,

the Hamiltonian reads $H_{\text{pol}} = \Delta_a a^\dagger a + \Delta_b b^\dagger b + g(a^\dagger b + b^\dagger a) + \Omega_a(e^{i\phi} a^\dagger + e^{-i\phi} a) + \Omega_b(b^\dagger + b) + \frac{U}{2} b^\dagger b^\dagger b b$, where $\Delta_{a,b} = \omega_{a,b} - \omega_L$ are the frequencies of cavity/exciton referred to the frequency of the laser ω_L that drives the photonic/excitonic field with amplitudes $\Omega_{a,b}$. The phase difference between them $\phi = \phi_a - \phi_b$ can be chosen such that $\phi_a = \phi$ and $\phi_b = 0$. The master equation for the dissipative dynamics of polaritons reads $\partial_t \rho = i[\rho, H_{\text{pol}}] + (\gamma_b/2)\mathcal{L}_b \rho + (\gamma_a/2)\mathcal{L}_a \rho$, where γ_a and γ_b are the decay rates of the photon and the exciton, respectively. As compared to the Jaynes–Cummings Hamiltonian (43), the polariton Hamiltonian substitutes the 2LS by a weakly interacting Bosonic mode, $b \rightarrow \sigma$ with nonlinearities $b^\dagger b^\dagger b b$, thus slightly displacing the state with two excitations while the 2LS forbids it entirely. In the case where $U \rightarrow \infty$, the Jaynes–Cummings limit is recovered, but in most experimental cases, U/γ_a is very small. In all cases, in the low driving regime ($\Omega_a \rightarrow 0$), the steady-state populations of the photon and the exciton are given by the same expressions as in the Jaynes–Cummings model, Equation (44) with $\sigma \rightarrow b$, since the 2LS converges to a bosonic field in the linear regime. The differences arise in the two-particle magnitudes (cf. Equation (45)).

$$g_a^{(2)} = \left\{ \begin{aligned} & [16g^4 + 8g^2(\gamma_a\gamma_b - 4\Delta_a\Delta_b) + \tilde{\Gamma}_a^2\tilde{\Gamma}_b^2] [\tilde{\Gamma}_b^2\tilde{\Gamma}_{11}^2(\gamma_b^2 + \tilde{U}_{12}^2) \\ & + 8g^2(U^2[4\Delta_b\tilde{\Delta}_{11} - \gamma_b\tilde{\gamma}_{11}] + 2\tilde{\Gamma}_{11}^2[\gamma_b^2 + \tilde{U}_{12}^2]\chi^2 \\ & + 8U\Delta_b^2\tilde{\Delta}_{11} - 2U\gamma_b^2\tilde{\Delta}_{13} - 4U\gamma_a\gamma_b\Delta_b) \\ & + 16g^4(U^2 + [\tilde{\gamma}_{11}^2 + (U + 2\tilde{\Delta}_{11})^2]\chi^4) \\ & - 16g\chi \cos \phi (\Delta_b\tilde{\Gamma}_{11}^2[\gamma_b^2 + 4\tilde{U}_{12}^2] + 2g^2[U(2\tilde{\Delta}_{11}\tilde{U}_{12} - \gamma_b\tilde{\gamma}_{11}) \\ & + (2U^2\tilde{\Delta}_{11} + 2\Delta_b\tilde{\Gamma}_{11}^2 + U\{\gamma_a\tilde{\gamma}_{11} + 4\tilde{\Delta}_{11}\tilde{\Delta}_{12}\})\chi^2]) \\ & + 8g^2\chi^2 \cos 2\phi (4g^2U[U + 2\tilde{\Delta}_{11}] - U^2[\gamma_b\tilde{\gamma}_{11} - 4\Delta_b\tilde{\Delta}_{11}] \\ & - [\gamma_b^2 - 4\Delta_b^2]\tilde{\Gamma}_{11}^2 + 2U[\gamma_a^2\Delta_b + \tilde{\Delta}_{12}(4\Delta_b\tilde{\Delta}_{11} - \gamma_b^2)]) \\ & - 8g\chi \sin \phi (\gamma_b\tilde{\Gamma}_{11}^2[\gamma_b^2 + \tilde{U}_{12}^2] + 4g^2[\gamma_b\tilde{\Gamma}_{11}^2\chi^2 \end{aligned} \right.$$

$$\begin{aligned}
 &+ U(\chi^2 - 1)(U\tilde{\gamma}_{11} + 2\gamma_b\Delta_a + 2\tilde{\gamma}_{12}\Delta_b)) \\
 &+ 8g^2\chi^2\sin 2\phi(-4g^2U\tilde{\gamma}_{11} + 4\gamma_b\Delta_b\tilde{\Gamma}_{11}^2 + 2U^2[\gamma_a\Delta_b + \gamma_b\tilde{\Delta}_{12}]) \\
 &+ U[\gamma_a^2\gamma_b + 4\gamma_b\tilde{\Delta}_{12}^2 + \gamma_a\tilde{\Gamma}_{11}^2]) \} / \{ (\tilde{\Gamma}_a^2\tilde{\Gamma}_{11}^2[\gamma_b^2 + \tilde{U}_{12}^2] \\
 &+ 16g^4[\tilde{\gamma}_{11}^2 + (U + 2\tilde{\Delta}_{11})^2] + 8g^2[U^2(\gamma_a\tilde{\gamma}_{11} - 4\Delta_a\tilde{\Delta}_{11}) \\
 &+ \tilde{\Gamma}_{11}^2(\gamma_a\gamma_b - 4\Delta_a\Delta_b) - 2U(\gamma_a^2\tilde{\Delta}_{11} - 2\gamma_a\gamma_b\Delta_b + 4\Delta_a\tilde{\Delta}_{11}\tilde{\Delta}_{12})]) \\
 &\times (4g^2\chi^2 + \tilde{\Gamma}_b^2 - 4g\chi[2\Delta_b\cos\phi + \gamma_b\sin\phi])^2 \} \quad (49a)
 \end{aligned}$$

$$\begin{aligned}
 g_b^{(2)} = &\{ \tilde{\Gamma}_{11}^2[16g^4 + 8g^2(\gamma_a\gamma_b - 4\Delta_a\Delta_b) + \tilde{\Gamma}_a^2\tilde{\Gamma}_b^2] \} / \\
 &\{ \tilde{\Gamma}_a^2\tilde{\Gamma}_{11}^2[\gamma_b^2 + \tilde{U}_{12}^2] + 16g^4[\tilde{\gamma}_{11}^2 + (U + 2\tilde{\Delta}_{11})^2] \\
 &+ 8g^2[U^2(\gamma_a\tilde{\gamma}_{11} - 4\Delta_a\tilde{\Delta}_{11}) + \tilde{\Gamma}_{11}^2(\gamma_a\gamma_b - 4\Delta_a\Delta_b) \\
 &- 2U(\gamma_a^2\tilde{\Delta}_{11} - 2\gamma_a\gamma_b\Delta_b + 4\Delta_a\tilde{\Delta}_{11}\tilde{\Delta}_{12})] \} \quad (49b)
 \end{aligned}$$

where we have used the short-hand notation $\gamma_+ = \gamma_a + \gamma_b$, $\Delta_{\pm} = \Delta_a \pm \Delta_b$ and $\Gamma_c^2 = \gamma_c^2 + 4\Delta_c^2$ for $c = a, b$, as well as $\tilde{\Delta}_{ij} \equiv i\Delta_a + j\Delta_b$, $\tilde{\gamma}_{ij} = i\gamma_a + j\gamma_b$, $\tilde{\Gamma}_{ij}^2 \equiv \tilde{\gamma}_{ij}^2 + 4\tilde{\Delta}_{ij}^2$, $\tilde{U}_{ij} = iU + j\Delta_b$ and \tilde{j} denotes negative integer values ($\tilde{j} = -j$). Note that a major conceptual difference with the Jaynes–Cummings model is that it now becomes relevant to consider the emitter (in this case, excitonic) two-photon coherence function, $g_b^{(2)}$, while in the Jaynes–Cummings case, one has the trivial result $g_{\sigma}^{(2)} = 0$. The exciton statistics enjoys noteworthy characteristics, as we shall shortly see.

We repeat in **Figure 11** the same plots for the polariton system as for the Jaynes–Cummings case (Figure 7). The applet^[124] also covers this more general case. The cavity population is exactly the same, as already mentioned, and all other panels bear clear analogies. The two-photon coherence function converges to the Jaynes–Cummings one in the infinite interaction limit ($\lim_{U \rightarrow \infty} g_a^{(2)}$) but is distinctly distorted for high-energy laser driving in the positive photon–exciton detuning region, and features an additional UA and CB couple of lines in the negative detuning region. The decomposition of $g_a^{(2)}$ as in Equation (6) can be made (the expressions are however bulky and not enlightening) and are shown in Figure 11d,e.

7.1. Conventional Statistics

Like in the Jaynes–Cummings model, one can identify the conventional antibunching (CA) and bunching (CB) by mapping the observed features to an underlying blockade mechanism, namely, the positions at which N -photon excitation occurs, which is when the laser is resonant with one of the states in the N -photon rung. The first rung that provides CA is given by the same Equation (46), with $N = 1$, since this corresponds to the linear regime where both systems converge. One finds, therefore, that the two CA blue lines in Figure 11a, marked in solid blue in (b), are the same as in the Jaynes–Cummings model. They coincide as well with the white regions in Figure 11c where the cavity emission

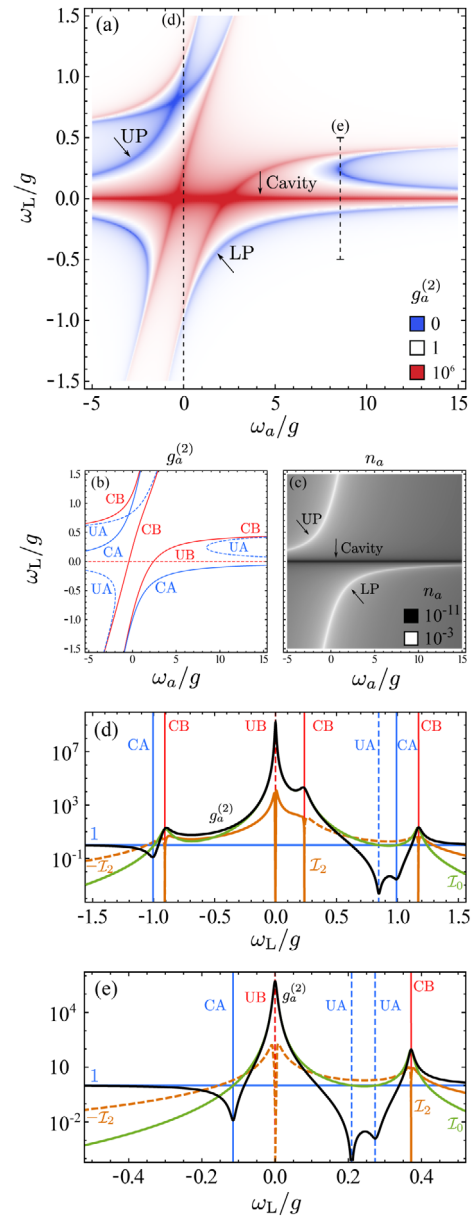


Figure 11. Polaritonic counterpart of Figure 7. a) $g_a^{(2)}$ and b) its structure in terms of conventional and unconventional features. CA (CB) is given by the resonant condition with the first (second) polariton manifold, cf. Equations (46) (for $N = 1$) and (50). UA is given by the interference condition Equation (51) and UB by $\omega_L = 0$. c) Population n_a and (d–e) $g_a^{(2)}$ (black line) for the two cuts shown in dashed lines in (a) with the cavity frequency either d) resonant with the 2LS or e) chosen to optimize UA ($\omega_a = 8.63g$). The decomposition in I_j components is also shown, with the same conventions as in Figure 7. Parameters: $\gamma_a = 0.1g$, $\gamma_b = 0.01g$, and $U = 10\gamma_a$.

is enhanced. This is the standard one-photon resonance, with a blockade of photons into higher rungs due to the non-linearity now introduced by the interactions (instead of the 2LS).

Higher rungs are different from the Jaynes–Cummings model, but their effects otherwise follow from the same principle and they are similarly obtained by diagonalizing the effective Hamiltonian in the corresponding N -excitation Hilbert

subspace, that is, in the basis $\{|N, 0\rangle, |N-1, 1\rangle, \dots, |0, N\rangle\}$ (where each state is characterized by the photon and exciton number). At the two-photon level, one is interested in the second rung, which contains three eigenstates. The expressions for the general eigenenergies are rather large but we can provide here the first order in the interactions U in the strong coupling limit ($g \gg \gamma_a, \gamma_b$)

$$E_0^{(2)} = \omega_a + \omega_b + \frac{g^2}{2R^2} U \quad (50a)$$

$$E_{\pm}^{(2)} = \omega_a + \omega_b \pm 2R + \frac{2g^2 + (\omega_a - \omega_b)[(\omega_a - \omega_b) \mp 2R]}{8R^2} U \quad (50b)$$

with $R = \sqrt{g^2 + (\omega_a - \omega_b)^2/4}$ the normal mode splitting typical of strong coupling. In this limit, $E_{\pm}^{(1)} = (\omega_a + \omega_b)/2 \pm R$. The CB lines are positioned, therefore, according to the conditions for two-photon excitation by the laser: $\omega_L = \text{Re}\{E_{\pm}^{(2)}\}/2$, $\text{Re}\{E_0^{(2)}\}/2$, $\text{Re}\{E_{\pm}^{(2)}\}/2$, in increasing order, as they appear in Figure 11a, marked with solid red lines in Figure 11b. The upper CB line, corresponding to $E_{+}^{(2)}$, is the faintest one in the cavity emission due to the fact that it has the most excitonic component. It is monotonically blueshifted with increasing U and becomes linear in the density plot as $E_{+}^{(2)} \rightarrow U$. The other two levels converge to those in the Jaynes–Cummings model in such case: $E_{-}^{(2)} \rightarrow -\sqrt{2}g$ and $E_0^{(2)} \rightarrow \sqrt{2}g$.

7.2. Unconventional Statistics

We now shift to the unconventional features in polariton blockade. Superbunching, or UB, is found by minimization of $\langle n_a \rangle$ and, therefore, also occurs for the same condition as the Jaynes–Cummings model $\Delta_b = \chi g \cos \phi$. Interestingly, the maximum superbunching is found at one of the crossings of UB and CB.

Now turning to the more interesting unconventional antibunching (UA) features, they are found, in the polariton case as well, from the minimization of $g_a^{(2)}$. Since the equations are quite bulky, only the case of cavity excitation ($\Omega_b = 0$) is included here. The UA curve is given by the solution of

$$\Delta_a = -\Delta_b - \frac{4g^2 \Delta_b}{\gamma_b^2 + 4\Delta_b^2} + \frac{2g^2(U + 2\Delta_b)}{\gamma_b^2 + (U + 2\Delta_b)^2} \quad (51)$$

and the conditions for perfect antibunching come from solving the equation

$$\gamma_b \left[1 + 4g^2 \left(-\frac{1}{\gamma_b^2 + 4\Delta_b^2} + \frac{1}{\gamma_b^2 + (U + 2\Delta_b)^2} \right) \right] = -\gamma_a \quad (52)$$

and subsequently imposing that every parameter must be real (or the more restrictive case: real and positive) that lead to additional restrictions.

As already noted, the polariton case adds a third CA line as compared to its Jaynes–Cummings counterpart. The correspondence between both cases is still clear, but this is largely thanks to the large interaction strength chosen in Figure 11, namely,

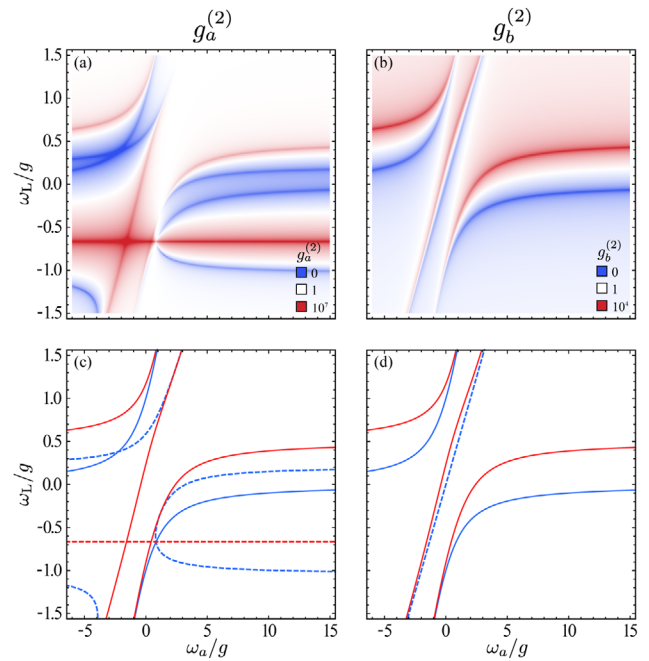


Figure 12. Effects on the polaritonic photon statistics. Same as Figure 11 but for a) nonzero exciton-driving and b) observed through the direct excitonic emission $g_b^{(2)}$. In the latter case, all the unconventional features have disappeared. The bottom row identifies the features through the structure of conventional and unconventional lines. Parameters: $\gamma_a = 0.1g$, $\gamma_b = 0.01g$, $\chi = 0$, and $U = 10\gamma_a$.

$U/\gamma_a = 10$. This choice will allow us to survey quickly the polaritonic phenomenology based on the more thoroughly discussed Jaynes–Cummings one. **Figure 12**, for instance, shows the polaritonic counterpart of Figure 8 on its left panel but for one case of mixed-pumping only, highlighting the considerable reshaping of the structure and the importance of controlling, or at least knowing, the ratio of exciton and photon driving. The right panel of Figure 12 provides $g_b^{(2)}$, which, if compared to Figure 11, shows that the main result is to remove all the unconventional features and retain only the conventional ones. There are also fewer peaks in the excitonic emission, producing a smoother background. Another dramatic feature of the excitonic correlations, which is apparent from Equation (49), is that it is independent from the ratio χ of driving, that is, the same result is obtained if driving the cavity alone, the exciton alone, or a mixture of both, in stark contrast with the cavity correlations (cf. Figures 11a and 12a where the only difference is that half the excitation drives the 2LS in the second case rather than going fully to the cavity in the first case). This could be of tremendous value for spectroscopic characterization of such systems since it is typically difficult to know the exact type of pumping, while experimental evidence shows that both fields are indeed being driven under coherent excitation.^[129] When measuring the excitonic correlations, there is no dependence from the particular type of coupling of the laser to the system. On the other hand, excitonic emission is much less straightforward of access. Also worthy of mention is that the crossing of the UA and CA lines already highlighted for the Jaynes–Cummings system as providing a high-quality

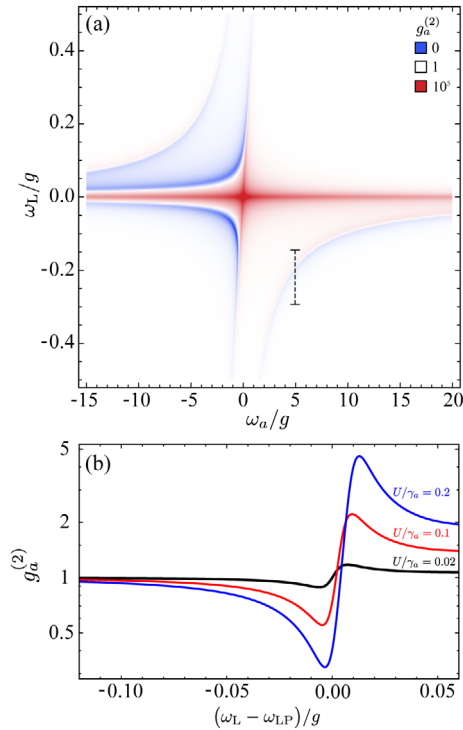


Figure 13. Polariton blockade. a) Same as Figure 11 but for an experimentally realistic weak value of $U/\gamma_a = 0.1$, showing how the UB and CA lines merge into the characteristic “polariton blockade” dispersive shape shown in red in panel (b) along the cut (dashed line) $\omega_a = 5g$ around the lower polariton branch ($\omega_{L,P} \approx -0.2g$). Also shown are similar dispersive shapes for other values of U/γ_a (black and blue curves).

and special type of antibunching also occurs there but without requiring both types of mixing.^[109] Note, finally, that one could similarly consider the lower and upper polariton statistics, but they are even less featureless, with correlations of the signal that merely follow the polariton branches.^[109]

Finally, in **Figure 13**, we focus on the effect of the interaction strength and how to optimize the observation of antibunching. We have already emphasized that for clarity of the connection between the Jaynes–Cummings and the polariton case, we have considered a value of U/γ_a substantially in excess even of the most generous estimates found in the literature.^[130] While it is not excluded that such a regime will be available in the near future, it is naturally more relevant to turn to the most common experimental configuration where $U/\gamma_a \ll 1$. We show such a case in Figure 13a, where $U/\gamma_a = 0.1$. We see how, as a result, the CB and CA lines of the positively detuned case collapse one onto the other. The UA line previously in between has, in the process, disappeared. The CA and CB however do not cancel each other but merge into a characteristic dispersive-like shape, shown in Figure 13b, the observation of which, predicted over a decade ago,^[27] has been a long-awaited result for polaritons and has indeed been just recently reported from two independent groups.^[38,39] While this shape has been regarded as an intrinsic and fundamental profile of polariton blockade, our wider picture shows how it arises instead from different features brought to close proximity by the weak interactions. The difficulty in reporting polariton

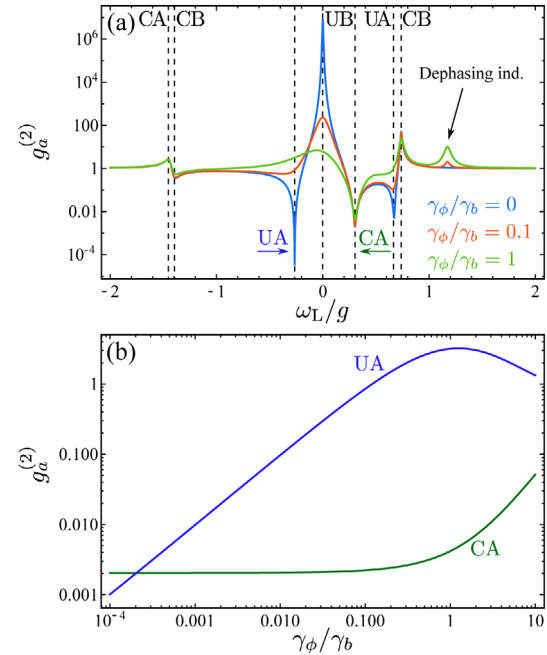


Figure 14. Effect of dephasing on conventional and unconventional statistics, illustrated with polaritons, but all systems behave similarly: unconventional features are fragile to dephasing as compared to conventional ones which are robust against it, as shown in two complementary ways for a) all resonances and b) as a function of dephasing for the UA & CA cases selected in (a). Conventional antibunching and remains essentially unaffected by dephasing rates that bring the unconventional one into bunching. Parameters: $\omega_a = -3g$, $\gamma_a = 0.1g$, $\gamma_\sigma = 0.01g$, and $U = g$.

blockade lies in the weak value of antibunching, which is largely due to the lack of knowledge of the full picture of photon correlations that we have now established. The current work indeed opens up the possibility to optimize antibunching over the full parameter space, and may be used to find parameters that would yield better antibunching for a particular set of experimental parameters, for instance by considering the intersection of UA and CA lines.^[109]

8. Dephasing

Conventional and unconventional statistics also differ in a fundamental way in their response to dephasing, which is a typical complication found particularly in the solid state. The simplest way to account for such an effect is to include to the master equation a term in the Lindblad form $(\gamma_\phi/2)\mathcal{L}_{\sigma^\dagger\sigma}\rho$ which describes pure dephasing at a rate γ_ϕ .^[131] Either from exact analytical results that can be obtained in some cases, such as for the two-level system,^[132] or from numerical simulations, it happens that, as a rule, unconventional features are fragile to dephasing, in the sense that resonances producing either bunching or antibunching, but most particularly those of strong antibunching that cancel exactly to first-order in the driving, are quickly spoiled by small values of dephasing. In contrast, conventional features are robust and the loss of antibunching becomes significant only when pure dephasing is a sizable fraction of radiative lifetimes. This is shown in **Figure 14** for the case of polaritons, but all other

platforms behave similarly. Figure 14a shows how the sharp resonances of UA and UB, that are theoretically zero and infinite respectively in the limit of vanishing driving, are basically washed away with a 10% dephasing rate only, in contrast to the CA resonance that remains essentially unaffected even when $\gamma_\phi \approx \gamma_\sigma$, as shown explicitly in Figure 14b where the UA and CA evolution is plotted for the full range of γ_ϕ . Note that the effect is so dramatic that the antibunching even turns to bunching in the unconventional case while it is still well below 0.1, so still an excellent value of antibunching, when $\gamma_\phi = 10\gamma_\sigma$ in the conventional case. This qualitative difference between the two cases is rooted in their respective mechanisms: as an interference effect, unconventional statistics are particularly sensitive to dephasing, since the slightest perturbation to the phase spoils destructive interferences. In contrast, conventional statistics follows from blockades or resonances with the level structure, which gets merely broadened by dephasing, and therefore still offering the same average conditions for the resonances. In fact, until dephasing alters the character of light–matter interactions, which happens when it gets very large through quenching or breaking correlators to yield rate equations instead of a coherent coupling, its effect on conventional antibunching is essentially negligible. Finally, although most resonances damp out with dephasing, note that one appears thanks to it (as seen on the right in Figure 14a), due to purely excitonic eigenstates acquiring a photonic component through dephasing and becoming bright.^[109]

9. Time-Dependence

So far, we have dealt exclusively with time-independent configurations and zero-delay correlators ($\tau = 0$). A feature in the time-dependent photon correlations has been observed since the revival of the unconventional mechanism by Liew and Savona^[32] and appears to be deeply connected to unconventional blockade: strong and rapid oscillations in $g^{(2)}(\tau)$. This came as a detrimental counterpart of the very small value at $\tau = 0$, since in the absence of a high time-precision, the averaging reduces the antibunching. Such oscillations are shown in Figure 15c in light green where they are contrasted with the conventional antibunching, dark green, that is far from being so strongly antibunched (log-scale inset) but is also much smoother. Oscillations are not, in fact, intrinsic to the mechanism, which can dispose of them.^[87] Although indeed related to unconventional antibunching, they are an indirect consequence rather than a necessary condition, being simply the result of a detuning between the homodyning field and the mode emitting the light, whose interference produces the unconventional statistics: the superposition of two waves with mismatched frequencies exhibits a beating, which yields these oscillations. One can thus expect to find them in all platforms, both for antibunching and bunching, as shown in Figure 15. In the self-homodyning version, where the system itself provides the coherent field to interfere with the quantum part of the signal in a way that optimizes the correlations, such a detuning can be simply the level-splitting from strong-coupling. This was the case in the original proposal,^[32] where oscillations are Rabi oscillations. In all cases, the suppression of oscillations can be achieved by getting rid of such a detuning. When the detuning comes from level-splitting, it may then seem unavoidable,

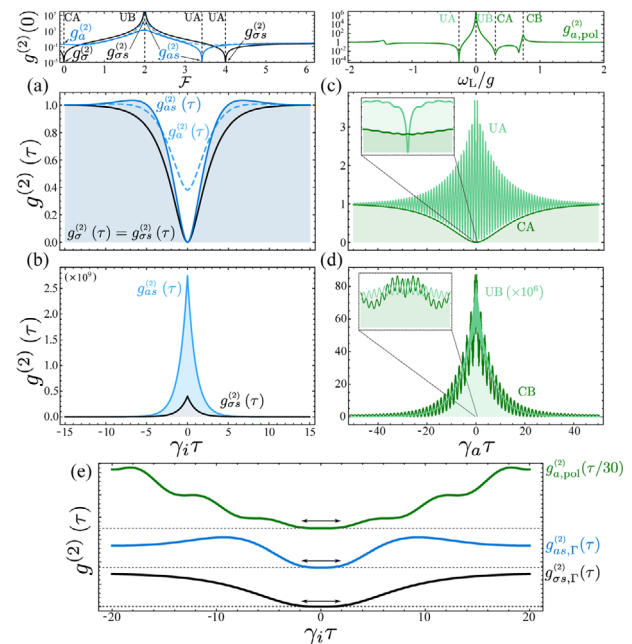


Figure 15. Time-dependence of two-photon correlations in the conventional and unconventional scenarios, with a 2LS and anharmonic oscillator (left column) and polaritons (right column), for both antibunching (middle row) and bunching (bottom row). The cases shown are those selected at the various points identified in the top-row for the resonances of the 2LS (black) and anharmonic oscillator (blue), labeling $g_s^{(2)}$ the homodyning case. a) Antibunching with and without homodyning and b) bunching (diverging to first-order in the driving) display no oscillations as compared to c) antibunching with polaritons in UA and CA, with strong oscillations as UA occurs with detuning between the driving laser and the emitting mode. Although likely to happen, this is not a per se feature of unconventional statistics. d) For bunching, oscillations are actually more prominent for the conventional mechanism. e) Plateaus around $\tau = 0$ (arrows) in frequency-filtered two-photon statistics from homodyning ($g_s^{(2)}$) or self-homodyning ($g^{(2)}$). The cases shown are for the 2LS (black), the anharmonic oscillator (blue), and polaritons (green). Parameters: $\Delta_\sigma = 0$ and $\Gamma/\gamma_\sigma = 0.5$ for the 2LS; $U/\gamma_a = 1$, $\Delta_\sigma/\gamma_a = \Delta_-$, and $\Gamma/\gamma_a = 0.5$ for the anharmonic system; $\gamma_a/g = 0.1$, $\gamma_b/g = 0.01$, $U/g = 1$, $\omega_a/g = -3$, and $\omega_L/g = 0.67$ for polaritons, with greatly reduced oscillations.

but in this case as well one can get rid of it through dissipative coupling,^[87] that is, a non-coherent, non-reversible type of coupling that does not dress the system. One still needs to bring an interfering mode, but since this can be done at resonance, this is an insightful way to free the strong antibunching of unconventional blockade from detuning oscillations.^[87] Figure 15 shows $g^{(2)}(\tau)$ for, on the one hand (left column), the anharmonic oscillator (in blue) and the two-level system (in black) as well as, on the other hand (right column), polaritons (in green, the Jaynes–Cummings system being essentially similar). The case of homodyning is still labeled *s*, as previously, but since the various platforms are now brought together, we maintain the emitter label as a subscript. Namely, for the two-level system, $g_{ss}^{(2)}$ is Equation (30) with $\mathcal{F} = 0$, while $g_{ss}^{(2)}$ is the same equation but with \mathcal{F}_2 and ϕ_2 given by Equation (31) with $N = 2$. For the anharmonic oscillator, $g_{as}^{(2)}$ is Equation (41) with $\Delta_b = \Delta_-$ and correcting field $\mathcal{F}_{2,1}$ and $\phi_{2,1}$ given by Equation (42), while $g_a^{(2)}$ is the same but with no

homodyning, that is, $\mathcal{F} = 0$. The polariton case $g_{a,\text{pol}}^{(2)}$, on the right-column, is given by Equation (49a). The time-dynamics for all these cases is shown in Figure 15a–d. These are lots of cases but that precisely display the same overall behaviour. Namely, when there is only one resonant frequency and the condition for antibunching and bunching can be found at zero (or almost zero) detuning with the laser (two-level system and anharmonic single mode), $g^{(2)}(\tau)$ does not oscillate. For the anharmonic mode, where detuning with the laser is not exactly zero (tending to zero as the nonlinearity increases), still some undulation is noticeable (Figure 15a in light blue solid line). On the other hand, the polariton scenario, where there are more eigenfrequencies involved, is more complex and varied. In the case where the laser is hitting a polariton branch, such as for CA, only that frequency is selected and no strong oscillations are present (dark green lines in Figure 15c). However, when the laser is completely out of resonance with the level structure, as is the case for UA (Figure 15c, light-green) and UB (Figure 15d, light-green), or at a resonance that involves more than one photon and levels, such as CB (where the laser is hitting a second-order two-photon resonance while not being far from to the first order one-photon resonances), oscillations appear more clearly (Figure 15d, dark green). In summary, oscillations have a common origin in both the conventional and unconventional scenario (mixing of different frequencies) with respective configurations being more (U) or less (C) prone to exhibit them.

Another, more subtle and less prominently featured characteristics found in time-dependent photon correlations is a plateau of antibunching, with a flat $g^{(2)}(\tau)$ that is produced around $\tau = 0$. Note that if $g^{(2)}(\tau)$ would be exactly zero over some finite interval, this would imply a time-gap in which no more than a single photon could ever be found, which realizes a perfect single photon source, as opposed to conventional types which merely reduce the probability of such occurrences. Such plateaus, however, result from several derivatives cancelling, but not all, since the functions are analytic, and $g^{(2)}$ is never strictly zero except at $\tau = 0$ and in the limit of vanishing driving. Since $g^{(2)}$ is a tricky^[133,134] measure of the single-photon character, the plateau of unconventional statistics is no guarantee of a qualitative change in single-photon emission, but it is the closest approximation so far to the ideal time-gapped scenario and its properties remain to be investigated. Its ubiquity throughout platforms is illustrated in Figure 15e where it is shown for the 2LS, $g_{\sigma_s, \Gamma}^{(2)}$, the anharmonic oscillator $g_{\sigma_a, \Gamma}^{(2)}$, and polaritons $g_a^{(2)}$. In the two former cases, the plateau is observed when frequency-filtering the signal in a frequency-window of width Γ .^[49,135] Although this plateau has been highlighted only recently,^[49] it can with hindsight be recognized in previous works.^[46] One can find it in higher-order correlators as well, for example, as a square-plateau in $g^{(3)}(\tau_1, \tau_2)$, but discussing this further here would bring us too far astray.

10. Discussion

We have now covered various aspects of the photon correlations from several coherently driven systems. At the heart of our description is the decomposition of the correlators into various terms that contribute to different orders in the driving. This al-

lows to identify the different mechanisms, which in agreement with the literature, can be termed conventional and unconventional. This also allows us to tune and optimize them. The skeleton of the structures can be found in closed-form to lowest order in the driving, which leads to exact zeros for antibunching and divergences for superbunching. Finite pumping merely distorts and damps out the corresponding resonances, that however provide the correct physical picture. The exact nature of the quantum states that are produced in this way remains to be fully clarified. In particular, the Gaussian-state approximation discussed in the literature holds to lower orders in the driving for the leading correlation functions only. For instance, for the case of the laser-corrected two-level system (Table 1), the squeezed-coherent Gaussian description holds up to the second-order in the driving for the population and to the first-order in the driving for $g^{(2)}$. Deviations occur for these observables to higher-orders in the driving, while higher-order correlation functions already differ to the lowest order in the driving. Such deviations seem to arise from the non-Gaussian nature of the quantum fluctuations in these highly non-linear systems. This remains to be investigated.

Such a general picture can nevertheless explain under a unified mechanism a wealth of observations that could otherwise appear to be peculiarities that are specific to a particular configuration. To take one recent example from a group that has been leading in the development and applications of the type of homodyning and self-homodyning discussed above, in ref. [101], Trivedi et al. studied the generalization of the Jaynes–Cummings system to N emitters: the so-called Tavis–Cummings Hamiltonian. Here, it is found that driving resonantly the eigenstates^[136] produces conventional antibunching, flanked by unconventional antibunching for laser frequencies detuned from the one- and two-photon resonances. This is the counterpart of the situation of Figures 7d (resonance) and 7e (detuning), both also shown in Figure 7a, where increasing N has the effect of bosonizing the interacting (matter-like) part of the system or decreasing the effective nonlinearity, similarly to decreasing g for $N = 1$. Interestingly, it is reported that while for the case of resonance, antibunching is spoiled with an increasing number of emitters N , in presence of a detuning, one of the antibunching peaks is, on the opposite, enhanced with increasing N . This apparently puzzling behavior is easily understood once the conventional and unconventional nature of the respective antibunching lines are recognized. In the resonant case, antibunching is always conventional, and as such it is reduced by the bosonization of the system due to its increasing number of emitters,^[137] or by reducing the coupling. Since both weaken the nonlinearity in the level structure, this destroys the conventional blockade that is based on it. With detuning, on the other hand, one finds not only conventional but also unconventional antibunching (cf. Figure 7b). Their CA is also reduced with increasing N , as reported, but their UA, however, increases, which can be expected since it is due to a self-homodyning interference between the coherent and incoherent parts of the emission at the two-photon level, as explained above, and this does not suffer from a reduced nonlinearity (or increasing N). It can in fact be also optimized (i.e., reduced) like all types of UA and as a result, should even reach $g^{(2)} = 0$ to lowest order for a proper choice of the detuning, that will depend on N in a way that remains to be computed. Since we have shown, however, that the interference nature of

UA makes it sensitive to dephasing, and that detuning^[132] results in fast oscillations in autocorrelation times, with a narrowing plateau of antibunching, one can also expect this antibunching to be particularly fragile and difficult to resolve when including a realistic model for its detection. This is consistent with the finding of ref. [101], that inhomogeneous broadening significantly reduces UA. Finally, they also find in both detuned and resonant cases the unconventional bunching, as the large bunching central peak that is a typical feature of the general mechanism (cf. Figure 7). This is therefore the super-chaotic noise due to self-homodyning stripping down the emission to its mere fluctuations. As such, the interpretation in terms of two-photon bound states that is offered in ref. [101] and in other works^[10,52] should be further analyzed and quantified. Possibly the emission in UB is less efficient for multiphoton physics as compared to leapfrog emission,^[128] due to the lack of a suppression mechanism for higher photon-number processes, and despite the large values of the correlation functions that they produce. This analysis could similarly be extended to other many-body photonic platforms, such as coupled-resonator arrays (see refs. [138–140] for reviews).

11. Summary and Conclusions

We have connected a hitherto disparate and voluminous phenomenology of photon statistics in the light emitted by a variety of optical systems into a unified picture that identifies two classes of conventional and unconventional features, covering both the cases of antibunching and bunching, which leads us to a classification of CA, UA, CB, and UB. One class (conventional), linked to real states repulsion, occurs at all orders and for all photon numbers while the other (unconventional) occurs for a given photon number with no a priori underlying level structure. To lowest order in the driving, the dynamical response can be described by interferences between a squeezed component and a coherent component, and thus, in this picture, one can understand the photon statistics emitted by many optical systems as simply arising from the particular way each implementation finds to produce some squeezing on the one hand and some coherent field on the other hand, and interfere them during its emission. To lowest order in the driving, the antibunching is exactly zero and superbunching becomes infinite for the unconventional mechanism. In agreement with the early literature, which foresaw the effect, we call this phenomenon “self-homodyning.” With this understanding, one can bring considerable tailoring of photon correlations by modifying the relative importance of coherence versus squeezing, which is conveniently achieved by superimposing a fraction of the driving laser to the output of the system (“homodyning”).

Acknowledgements

This article is part of a special series highlighting advances in quantum science and technology.

Conflict of Interest

The authors declare no conflict of interest.

Keywords

antibunching, blockade, photon correlations, photon statistics, squeezing, superbunching, unconventional photon blockade

- [1] R. J. Glauber, *Rev. Mod. Phys.* **2006**, *78*, 1267.
- [2] R. H. Brown, R. C. Jennison, M. K. D. Gupta, *Nature* **1952**, *170*, 1061.
- [3] R. H. Brown, R. Q. Twiss, *Nature* **1956**, *178*, 1447.
- [4] H. J. Kimble, M. Dagenais, L. Mandel, *Phys. Rev. Lett.* **1977**, *39*, 691.
- [5] A. İmamoglu, Y. Yamamoto, *Phys. Rev. Lett.* **1994**, *72*, 210.
- [6] M. J. Werner, A. İmamoglu, *Phys. Rev. A* **1999**, *61*, 011801(R).
- [7] J. Kim, O. Benson, H. Kan, Y. Yamamoto, J. Kim, O. Benson, H. Kan, Y. Yamamoto, *Nature* **1999**, *397*, 500.
- [8] P. Michler, A. Kiraz, C. Becher, W. V. Schoenfeld, P. M. Petroff, L. Zhang, E. Hu, A. İmamoglu, *Science* **2000**, *290*, 2282.
- [9] K. Birnbaum, A. Boca, R. Miller, A. Boozer, T. Northup, H. Kimble, *Nature* **2005**, *436*, 87.
- [10] A. Faraon, I. Fushman, D. Englund, N. Stoltz, P. Petroff, J. Vucković, *Nature Phys.* **2008**, *4*, 859.
- [11] B. Dayan, A. S. Parkins, T. Aoki, E. P. Ostby, K. J. Vahala, H. J. Kimble, *Science* **2008**, *319*, 1062.
- [12] C. Lang, D. Bozyigit, C. Eichler, L. Steffen, J. M. Fink, A. A. Abdumalikov Jr., M. Baur, S. Philipp, M. P. da Silva, A. Blais, A. Wallraff, *Phys. Rev. Lett.* **2011**, *106*, 243601.
- [13] A. J. Hoffman, S. J. Srinivasan, S. Schmidt, L. Spietz, J. Aumentado, H. E. Türeci, A. A. Houck, *Phys. Rev. Lett.* **2011**, *107*, 053602.
- [14] I. G. Kaplan, *The Pauli Exclusion Principle: Origin, Verifications and Applications*, Wiley-Blackwell, Hoboken, NJ **2016**.
- [15] M. Massimi, *Pauli's Exclusion Principle: The Origin and Validation of a Scientific Principle*, Cambridge University Press, Cambridge **2005**.
- [16] D. V. Averin, K. K. Likharev, *J. Low Temp. Phys.* **1986**, *62*, 345.
- [17] T. A. Fulton, G. J. Dolan, *Phys. Rev. Lett.* **1987**, *59*, 109.
- [18] M. A. Kastner, *Phys. Today* **1993**, *46*, 24.
- [19] E. Urban, T. A. Johnson, T. Henage, L. Isenhower, D. D. Yavuz, T. G. Walker, M. Saffman, *Nature Phys.* **2009**, *5*, 110.
- [20] A. Gaëtan, Y. Miroshnychenko, T. Wilk, A. Chotia, M. Viteau, D. Comparat, P. Pillet, A. Browaeys, P. Grangier, *Nature Phys.* **2009**, *5*, 115.
- [21] A. İmamoglu, H. Schmidt, G. Woods, M. Deutsch, *Phys. Rev. Lett.* **1997**, *79*, 1467.
- [22] I. Carusotto, *Phys. Rev. A* **2001**, *63*, 023610.
- [23] P. Rabl, *Phys. Rev. Lett.* **2011**, *107*, 063601.
- [24] D. Sanvitto, F. Laussy, D. Gerace, *Nature Mater.* **2019**, *18*, 200.
- [25] P. D. Drummond, D. F. Walls, *J. Phys. A: Math. Gen.* **1980**, *13*, 725.
- [26] A. Kavokin, J. J. Baumberg, G. Malpuech, F. P. Laussy, *Microcavities*, 2nd ed., Oxford University Press, Oxford **2017**.
- [27] A. Verger, C. Ciuti, I. Carusotto, *Phys. Rev. B* **2006**, *73*, 193306.
- [28] O. E. Daïf, A. Baas, T. Guillet, J. P. Brantut, R. I. Kaitouni, J. L. Staehli, F. Morier-Genoud, B. Deveaud, *Appl. Phys. Lett.* **2006**, *88*, 061105.
- [29] I. Rosenberg, D. Liran, Y. Mazuz-Harpaz, K. West, L. Pfeiffer, R. Rapaport, *Sci. Adv.* **2018**, *4*, eaat8880.
- [30] E. Togan, H. T. Lim, S. Faelt, W. Wegscheider, A. İmamoglu, *Phys. Rev. Lett.* **2018**, *121*, 227402.
- [31] N. Jia, A. Georgakopoulos, A. Ryou, N. Schine, A. Sommer, J. Simon, *Phys. Rev. A* **2016**, *93*, 041802(R).
- [32] T. C. H. Liew, V. Savona, *Phys. Rev. Lett.* **2010**, *104*, 183601.
- [33] M. Bamba, A. İmamoglu, I. Carusotto, C. Ciuti, *Phys. Rev. A* **2011**, *83*, 021802(R).
- [34] M. A. Lemonde, N. Didier, A. A. Clerk, *Phys. Rev. A* **2014**, *90*, 063824.
- [35] H. J. Carmichael, *Phys. Rev. Lett.* **1985**, *55*, 2790.
- [36] H. J. Carmichael, R. J. Brecha, P. R. Rice, *Opt. Commun.* **1991**, *82*, 73.
- [37] G. T. Foster, S. L. Mielke, L. A. Orozco, *Phys. Rev. A* **2000**, *61*, 053821.

- [38] A. Delteil, T. Fink, A. Schade, S. Höfling, C. Schneider, A. İmamoglu, *Nature Mater.* **2019**, *18*, 219.
- [39] G. Muñoz-Matutano, A. Wood, M. Johnson, X. V. Asensio, B. Baragiola, A. Reinhard, A. Lemaître, J. Bloch, A. Amo, B. Besga, M. Richard, T. Volz, *Nature Mater.* **2019**, *18*, 213.
- [40] C. Vaneph, A. Morvan, G. Aiello, M. Féchant, M. Aprili, J. Gabelli, J. Estève, *Phys. Rev. Lett.* **2018**, *121*, 043602.
- [41] H. Snijders, J. Frey, J. Norman, H. Flayac, V. Savona, A. Gossard, J. Bowers, M. van Exter, D. Bouwmeester, W. Löffler, *Phys. Rev. Lett.* **2018**, *121*, 043601.
- [42] S. Ferretti, D. Gerace, *Phys. Rev. B* **2012**, *85*, 033303.
- [43] S. Ferretti, L. C. Andreani, H. E. Türeci, D. Gerace, *Phys. Rev. A* **2010**, *82*, 013841.
- [44] S. Ferretti, V. Savona, D. Gerace, *New J. Phys.* **2013**, *15*, 025012.
- [45] H. Flayac, V. Savona, *Phys. Rev. A* **2013**, *88*, 033836.
- [46] H. Flayac, V. Savona, *Phys. Rev. A* **2016**, *94*, 013815.
- [47] H. Flayac, V. Savona, *Phys. Rev. A* **2017**, *95*, 043838.
- [48] X. Liang, Z. Duan, Q. Guo, C. Liu, Y. R. S. Guan, Y. Ren, *Phys. Rev. A* **2019**, *100*, 063834.
- [49] J. C. López Carreño, E. Zubizarreta Casalengua, E. del Valle, F. P. Laussy, *Quantum Sci. Technol.* **2018**, *3*, 045001.
- [50] K. A. Fischer, K. Müller, A. Rundquist, T. Sarmiento, A. Y. Piggott, Y. Kelaita, C. Dory, K. G. Lagoudakis, J. Vucković, *Nature Phys.* **2016**, *10*, 163.
- [51] K. Müller, K. A. Fischer, C. Dory, T. Sarmiento, K. G. Lagoudakis, A. Rundquist, Y. A. Kelaita, J. Vucković, *Optica* **2016**, *3*, 931.
- [52] C. Dory, K. A. Fischer, K. Müller, K. G. Lagoudakis, T. Sarmiento, A. Rundquist, J. L. Zhang, Y. Kelaita, N. V. Saprà, J. Vucković, *Phys. Rev. A* **2017**, *95*, 023804.
- [53] K. Fischer, S. Sun, D. Lukin, Y. Kelaita, R. Trivedi, J. Vucković, *Phys. Rev. A* **2018**, *98*, 021802(R).
- [54] K. A. Fischer, Y. A. Kelaita, N. V. Saprà, C. Dory, K. G. Lagoudakis, K. Müller, J. Vucković, *Phys. Rev. Appl.* **2017**, *7*, 044002.
- [55] J. Li, Y. Wu, *Phys. Rev. A* **2018**, *98*, 053801.
- [56] M. Van Regemortel, S. Ravets, A. İmamoglu, I. Carusotto, M. Wouters, *SciPost* **2018**, *5*, 013.
- [57] X. Xu, Y. Li, *Phys. Rev. A* **2014**, *90*, 043822.
- [58] H. Snijders, J. A. Frey, J. Norman, M. P. Bakker, E. C. Langman, A. Gossard, J. E. Bowers, M. P. van Exter, D. Bouwmeester, W. Löffler, *Nature Comm.* **2016**, *7*, 12578.
- [59] W. Zhang, Z. Yu, Y. Liu, Y. Peng, *Phys. Rev. A* **2014**, *89*, 043832.
- [60] J. Tang, W. Geng, X. Xu, *Sci. Rep.* **2015**, *5*, 9252.
- [61] H. Z. Shen, Y. H. Zhou, X. X. Yi, *Phys. Rev. A* **2015**, *91*, 063808.
- [62] H. Z. Shen, Y. H. Zhou, H. D. Liu, G. C. Wang, X. X. Yi, *Opt. Express* **2015**, *23*, 32835.
- [63] J. Li, R. Yu, Y. Wu, *Phys. Rev. A* **2015**, *92*, 053837.
- [64] X. W. Xu, Y. J. Li, *J. Phys. B.: At. Mol. Phys.* **2013**, *46*, 035502.
- [65] X. W. Xu, A. X. Chen, Y. Liu, *Phys. Rev. A* **2016**, *94*, 063853.
- [66] X. Wang, A. Miranowicz, H. R. Li, F. Nori, *Phys. Rev. A* **2016**, *93*, 063861.
- [67] G. Wang, H. Z. Shen, C. Sun, C. Wu, J. L. Chen, K. Xue, *J. Mod. Opt.* **2017**, *64*, 583.
- [68] X. Cheng, H. Ye, Z. Yu, *Superlatt. Microstruct.* **2017**, *105*, 81.
- [69] W. W. Deng, G. X. Li, H. Qin, *Opt. Express* **2017**, *6*, 6767.
- [70] B. Zhou, G. Li, *Phys. Rev. A* **2016**, *94*, 033809.
- [71] Y. L. Liu, G. Z. Wang, Y. Liu, F. Nori, *Phys. Rev. A* **2016**, *93*, 013856.
- [72] G. Y. Kryuchkyan, A. R. Shahinyan, I. A. Shelykh, *Phys. Rev. A* **2016**, *93*, 043857.
- [73] Y. H. Zhou, H. Z. Shen, X. Q. Shao, X. X. Yi, *Opt. Express* **2016**, *24*, 17332.
- [74] Y. Yu, H. Y. Liu, *J. Mod. Opt.* **2017**, *64*, 1342.
- [75] Y. H. Zhou, H. Z. Shen, X. Y. Zhang, X. X. Yi, *Phys. Rev. A* **2018**, *97*, 043819.
- [76] D. Gerace, H. E. Türeci, A. İmamoglu, V. Giovannetti, R. Fazio, *Nature Phys.* **2009**, *5*, 281.
- [77] H. Flayac, V. Savona, *Phys. Rev. A* **2017**, *96*, 053810.
- [78] A. Kubanek, A. Ourjoumtsev, I. Schuster, M. Koch, P. W. H. Pinkse, K. Murr, G. Rempe, *Phys. Rev. Lett.* **2008**, *101*, 203602.
- [79] A. Maser, B. Gmeiner, T. Utikal, S. Götzinger, V. Sandoghdar, *Nature Photon.* **2016**, *10*, 450.
- [80] X. L. Chu, S. Götzinger, V. Sandoghdar, *Nature Photon.* **2017**, *11*, 58.
- [81] D. Wang, H. Kelkar, D. Martin-Cano, D. Rattenbacher, A. Shkarin, T. Utikal, S. Götzinger, V. Sandoghdar, *Nature Phys.* **2019**, *15*, 483.
- [82] N. Jia, N. Schine, A. Georgakopoulos, A. Ryou, L. W. Clark, A. Sommer, J. Simon, *Nature Phys.* **2018**, *14*, 550.
- [83] K. Müller, A. Rundquist, K. A. Fischer, T. Sarmiento, K. G. Lagoudakis, Y. A. Kelaita, C. Sánchez Muñoz, E. del Valle, F. P. Laussy, J. Vucković, *Phys. Rev. Lett.* **2015**, *114*, 233601.
- [84] A. J. Bennett, J. P. Lee, D. J. P. Ellis, T. Meany, E. Murray, F. F. Floether, J. P. Griffiths, I. Farrer, D. A. Ritchie, A. J. Shields, *Sci. Adv.* **2016**, *2*, e1501256.
- [85] D. Najer, I. Söllner, P. Sekatski, V. Dolique, M. C. Löbl, D. Riedel, R. Schott, S. Starosielec, S. R. Valentin, A. D. Wieck, N. Sangouard, A. Ludwig, R. J. Warburton, *Nature* **2019**, *575*, 622.
- [86] Y. Liu, X. Xu, A. Miranowicz, F. Nori, *Phys. Rev. A* **2014**, *89*, 043818.
- [87] H. Flayac, D. Gerace, V. Savona, *Sci. Rep.* **2015**, *5*, 11223.
- [88] S. Ghosh, T. C. Liew, *Phys. Rev. Lett.* **2019**, *123*, 013602.
- [89] H. Z. Shen, C. Shang, Y. H. Zhou, X. X. Yi, *Phys. Rev. Lett.* **2018**, *98*, 023856.
- [90] I. Pietikäinen, J. Tuorila, D. S. Golubev, G. S. Paraoanu, *Phys. Rev. A* **2019**, *99*, 063828.
- [91] A. Majumdar, M. Bajcsy, A. Rundquist, J. Vucković, *Phys. Rev. Lett.* **2012**, *108*, 183601.
- [92] O. Kyriienko, T. C. H. Liew, *Phys. Rev. A* **2014**, *90*, 063805.
- [93] O. Kyriienko, E. A. Ostrovskaya, O. A. Egorov, I. A. Shelykh, T. C. H. Liew, *Phys. Rev. B* **2014**, *90*, 125407.
- [94] B. Sarma, A. K. Sarma, *Phys. Rev. A* **2017**, *96*, 053827.
- [95] A. Majumdar, D. Gerace, *Phys. Rev. B* **2013**, *87*, 235319.
- [96] D. Gerace, V. Savona, *Phys. Rev. A* **2014**, *89*, 031803(R).
- [97] Y. H. Zhou, H. Z. Shen, X. X. Yi, *Phys. Rev. A* **2015**, *92*, 023838.
- [98] H. Q. Shi, X. W. Xu, N. H. Liu, *Sci. Rep.* **2019**, *9*, 8754.
- [99] M. Bajcsy, A. Majumdar, A. Rundquist, J. Vucković, *New J. Phys.* **2013**, *15*, 025014.
- [100] M. Radulaski, K. A. Fischer, K. G. Lagoudakis, J. L. Zhang, J. Vucković, *Phys. Rev. A* **2017**, *96*, 011801(R).
- [101] R. Trivedi, M. Radulaski, K. A. Fischer, S. Fan, J. Vucković, *Phys. Rev. Lett.* **2019**, *122*, 243602.
- [102] J. C. Loredó, C. Antón, B. Reznichenko, P. Hilaire, A. Harouri, C. Millet, H. Ollivier, N. Somaschi, L. D. Santis, A. Lemaître, I. Sagnes, L. Lanco, A. Auffèves, O. Krebs, P. Senellart, *Nature Photon.* **2019**, *13*, 803.
- [103] M. Knap, E. Arrigoni, W. von der Linden, J. H. Cole, *Phys. Rev. A* **2011**, *83*, 023821.
- [104] P. Schwendimann, A. Quattropani, *Phys. Rev. A* **2012**, *86*, 043811.
- [105] D. G. Angelakis, M. F. Santos, S. Bose, *Phys. Rev. A* **2007**, *76*, 031805.
- [106] T. Grujic, S. R. Clark, D. Jaksch, D. G. Angelakis, *Phys. Rev. A* **2013**, *87*, 053846.
- [107] W. Casteels, C. Ciuti, *Phys. Rev. A* **2017**, *95*, 013812.
- [108] T. Ozawa, H. M. Price, A. Amo, N. Goldman, M. Hafezi, L. Lu, M. C. Rechtsman, D. Schuster, J. Simon, O. Zilberberg, I. Carusotto, *Rev. Mod. Phys.* **2019**, *91*, 015006.
- [109] E. Zubizarreta Casalengua, J. C. López Carreño, F. P. Laussy, E. del Valle, arXiv:2004.11885.
- [110] L. Mandel, *Phys. Rev. Lett.* **1982**, *49*, 136.
- [111] W. Vogel, *Phys. Rev. Lett.* **1991**, *67*, 2450.
- [112] W. Vogel, *Phys. Rev. A* **1995**, *51*, 4160.

- [113] C. H. H. Schulte, J. Hansom, A. E. Jones, C. Matthiesen, C. L. Gall, M. Atatüre, *Nature* **2015**, 525, 222.
- [114] B. Kühn, W. Vogel, M. Mraz, S. Köhnje, B. Hage, *Phys. Rev. Lett.* **2017**, 118, 153601.
- [115] C. C. Gerry, P. L. Knight, *Introductory Quantum Optics*, Cambridge University Press, Cambridge **2005**.
- [116] J. C. López Carreño, E. Zubizarreta Casalengua, E. del Valle, F. P. Laussy, arXiv:1610.06126 **2016**.
- [117] E. del Valle, F. P. Laussy, *Phys. Rev. A* **2011**, 84, 043816.
- [118] J. Dalibard, S. Reynaud, *J. Phys. France* **1983**, 44, 1337.
- [119] B. R. Mollow, *Phys. Rev.* **1969**, 188, 1969.
- [120] R. Loudon, *The Quantum Theory of Light*, 3rd ed., Oxford Science Publications, Oxford **2000**.
- [121] P. M. Visser, G. Nienhuis, *Phys. Rev. A* **1995**, 52, 4727.
- [122] E. Jaynes, F. Cummings, *Proc. IEEE* **1963**, 51, 89.
- [123] B. W. Shore, P. L. Knight, *J. Mod. Opt.* **1993**, 40, 1195.
- [124] E. Zubizarreta Casalengua, J. C. López Carreño, F. P. Laussy, E. del Valle, Polariton and Jaynes-Cummings Blockade, <http://demonstrations.wolfram.com/PolaritonAndJaynesCummingsBlockade/> (accessed: January 2019).
- [125] E. del Valle, F. P. Laussy, C. Tejedor, *Phys. Rev. B* **2009**, 79, 235326.
- [126] F. P. Laussy, E. del Valle, M. Schrapp, A. Laucht, J. J. Finley, *J. Nanophoton.* **2012**, 6, 061803.
- [127] Equation (48) generalizes the condition given in ref. [35] for the resonant case and coincides with it with the notation $\gamma_a/2 \rightarrow \kappa$ and $\mathcal{C} \rightarrow \mathcal{C}/2$.
- [128] C. Sánchez Muñoz, E. del Valle, A. G. Tudela, K. Müller, S. Lichtmannecker, M. Kaniber, C. Tejedor, J. Finley, F. Laussy, *Nature Photon.* **2014**, 8, 550.
- [129] L. Dominici, D. Colas, S. Donati, J. P. R. Cuartas, M. D. Giorgi, D. Ballarini, G. Guirales, J. C. López Carreño, A. Bramati, G. Gigli, E. del Valle, F. P. Laussy, D. Sanvitto, *Phys. Rev. Lett.* **2014**, 113, 226401.
- [130] Y. Sun, Y. Yoon, M. Steger, G. Liu, L. N. Pfeiffer, K. West, D. W. Snoke, K. A. Nelson, *Nature Phys.* **2017**, 13, 870.
- [131] G. S. Agarwal, S. D. Gupta, *Phys. Rev. A* **1990**, 42, 1737.
- [132] J. C. López Carreño, E. Zubizarreta Casalengua, F. P. Laussy, E. del Valle, *J. Phys. B: At. Mol. Phys.* **2019**, 52, 035504.
- [133] E. Zubizarreta Casalengua, J. C. López Carreño, E. del Valle, F. P. Laussy, *J. Math. Phys.* **2017**, 58, 062109.
- [134] P. Grünwald, *New J. Phys.* **2019**, 21, 093003.
- [135] E. del Valle, A. González-Tudela, F. P. Laussy, C. Tejedor, M. J. Hartmann, *Phys. Rev. Lett.* **2012**, 109, 183601.
- [136] F. Laussy, A. Laucht, E. del Valle, J. J. Finley, J. M. Villas-Bôas, *Phys. Rev. B* **2011**, 84, 195313.
- [137] R. H. Dicke, *Phys. Rev.* **1954**, 93, 99.
- [138] M. J. Hartmann, F. G. S. L. Brandão, M. B. Plenio, *Nature Phys.* **2006**, 2, 849.
- [139] A. D. Greentree, C. Tahan, J. H. Cole, L. C. L. Hollenberg, *Nature Phys.* **2006**, 2, 856.
- [140] C. Noh, D. G. Angelakis, *Rep. Prog. Phys.* **2017**, 80, 016401.